molecular pharmaceutics

pubs.acs.org/molecularpharmaceutics

Article

Multiscale Diffusion, Dynamic Cluster Formation, and Intermolecular Interactions in Pharmaceutically Relevant Monoclonal Antibody Formulations

Ilaria Mosca,* Christian Beck, Laura Mateo-Miñarro, Roody Nasro, Anna Carlotta Grundel, Ingo Hoffmann, Kévin Pounot, Olga Matsarskaia, Christoph Grapentin, Tilo Seydel,* and Frank Schreiber*

Cite This: *Mol. Pharmaceutics* 2025, 22, 5373−5388

Read Online

ACCESS | Metrics & More | Article Recommendations | Supporting Information

ABSTRACT: Due to their specificity and versatility, monoclonal antibodies (mAbs) are the most popular class of biopharmaceuticals typically administered via intravenous injection. One of the current pharmaceutical challenges concerns mAb formulations for subcutaneous (SC) injection, which is gaining importance as an alternative administration route offering convenience to patients by allowing self-administration compared to other parenteral delivery methods. With volumes lower than 1−2 mL being better tolerated in the subcutaneous space, highly concentrated mAb formulations are needed to achieve significant therapeutic effects, potentially increasing the solution viscosity and altering drug injectability. The main challenge is to maintain the solution viscosity below the SC injectability threshold (15−20 mPa·s) while preserving solution stability. Since the understanding of macroscopic viscosity requires in-depth knowledge on protein multiscale diffusion, mutual interactions, and aggregation, we employ two complementary neutron scattering techniques to investigate 9 different mAbs of IgG1/IgG4 subtypes in aqueous solution as a function of protein concentration and temperature. The synergy between neutron spin-echo (NSE), a spectroscopy technique providing dynamic information, and small-angle neutron scattering (SANS), a time-averaged static technique, enables us to probe the short-time collective diffusion of different mAbs, explore their self-association into small transient clusters, their intermolecular interactions, and ultimately access their internal dynamics. This study builds on previous neutron backscattering (NBS) findings, bridging a critical gap between the time scales probed by NBS and viscometry. It also confirms that the formation of short-lived clusters comprising more than two monomers is a key factor driving high solution viscosity, phase separation, and opalescence.

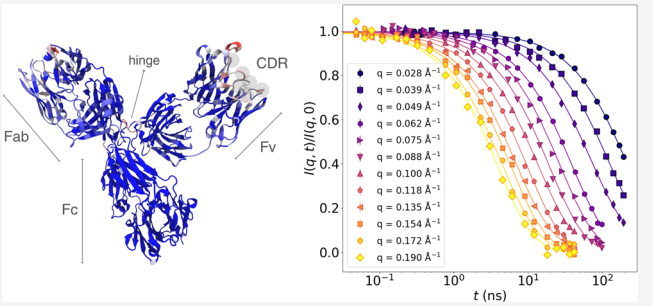

KEYWORDS: *monoclonal antibodies, self-association, viscosity, collective diffusion, neutron spin-echo spectroscopy, small-angle neutron scattering, intermolecular interactions, transient clusters*

1. INTRODUCTION

1.1. Scientific Relevance. When Köhler and Milstein developed the Nobel Prize winning hybridoma technology in the 1970s,[1] it was not immediately obvious at that time that monoclonal antibodies (mAbs) would become the most popular class of biopharmaceuticals. This technology was employed to develop Orthoclone OKT3 (muromonab-CD3), which became the first monoclonal antibody approved by the U.S. Food and Drug Administration (FDA).[2] Since that time, antibody therapeutics research and development have experienced remarkable growth, especially in the last two decades. Until the end of 2023, nearly 200 mAbs in total have received approval in the U.S. or other countries,[3] with 13 new ones in 2023,[4] 21 in 2024,[5,6] and more are forecast to be either approved or to enter regulatory reviews by the end of 2025.[6] The already broad spectrum of clinical applications of these biopharmaceuticals is currently expanding and includes the treatment of several types of cancers,[7−9] infectious and autoimmune diseases,[10,11] multiple sclerosis,[12] kidney diseases,[13] migraine,[14,15] and the prevention of malaria.[16] In the last two decades, the development of mAbs for the treatment of neurodegenerative pathologies such as Alzheimer's disease has been the subject of an extensive research,[17−20] but still a lot of work has to be done for substantial steps forward.[21,22]

Received: March 12, 2025
Revised: August 11, 2025
Accepted: August 11, 2025
Published: August 19, 2025

1.2. Motivation. Due to the extremely acidic environment of the gastrointestinal tract and mostly to the challenges related to absorption and biodistribution via this route, monoclonals cannot be administered orally without suitable delivery vehicles.[23] Therefore, the more suitable route is parenteral administration via intravenous (IV) or subcutaneous (SC) injections. Whereas IV refers to injecting the drugs directly into the blood vessels, with SC the substance is injected into the subcutaneous space. IV administration is normally performed in hospitals by specialized personnel, which is not always practical and a limiting factor for patients suffering from chronic diseases and requiring life-long treatment. In recent years, pharmaceutical research has been working to engineer and produce antibody formulations specific for SC injection[24,25] in order to enable patients to benefit from self-administration and more flexibility.[26−28] Moreover, SC administration allows a sustained systemic availability of the drug due to slower transfer from subcutaneous tissue (into blood) and reduced side effects due to avoidance of concentration peaks.

Since the amount of antibody needed to achieve a significant therapeutic effect is around hundreds of milligrams and the injectable volume in the subcutaneous space is in the range of 0.5−2 mL, this administration route requires high concentrations (in the 100−200 mg/mL range), potentially leading to viscosities exceeding a tolerance threshold of ∼15 to 20 mPa·s (or cP).[29,30] This translates into high injection forces or long injection times.[24,31] In addition to rendering the drug administration being painful or difficult (and sometimes impossible), high viscosity may also compromise the physicochemical stability of these pharmaceuticals before, during, and after the injection.[32,33] Since the procedure of SC injection alone overall reduces the physicochemical stability of mAbs,[34] controlling their solution viscosity is of great interest. To this end, several studies on the microscopic origin of macroscopic viscosity of highly concentrated mAb solutions have been conducted to optimize their design and manufacturability[35,36] by attempting to reach a fundamental understanding of this phenomenon and, ultimately, to design strategies for viscosity reduction.

1.3. State of the Art. Proteins in solution, especially antibodies, may undergo reversible self-association (RSA) and potential irreversible aggregation, two dissimilar processes in terms of physicochemical properties,[37−39] but equally concerning issues for manufacturability. RSA has been identified as one of the main reasons for high viscosity in mAb solutions[40,41] and can be influenced by multiple parameters including concentration, pH, temperature, ionic strength,[40] or specific interactions between protein domains.[42,43] On a macroscopic level, RSA strongly impacts the visual appearance of antibody solutions, causing opalescence, increased turbidity, and even phase separation.[44−50] Both electrostatic and hydrophobic protein−protein interactions (PPIs) seem to play a role in driving RSA[51] and thus in increasing solution viscosity. As a result, minimizing protein self-interactions is the key for viscosity reduction, and it can be achieved through two complementary approaches: protein engineering and formulation optimization.

Protein engineering is usually the first explored route for viscosity reduction based on applying small modifications in the antibody primary sequence and predicting how the viscosity is affected by those. Kastelic et al. found that different viscosity trends depend on how different mAb binding sites—Fab (antigen-binding fragment (Fabs)) and Fc (crystallizable fragment, cf. Figure 1)—contribute to aggregation, showing

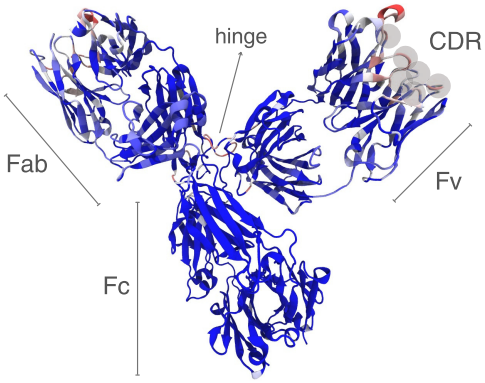

Figure 1. Structure of an IgG4 mAb and sequence similarity with IgG1 mAbs. The sequences of the mAbs were aligned using VMD[60] "MultiSeq" module[61] with ClustalW algorithm[62] and their results shown by sequence similarity using BLOSUM100. Sequence similarity is shown directly in the structure of mAb4* (IgG4) and represented with a color ranging from blue for high similarity to red for low similarity. The graphic was rendered with "NewCartoon" style. The different mAbs under study show almost identical structures in the Fc region, while they differ in their variable domain Fv, especially in the six complementarity determining regions (CDR) loops (or hypervariable regions, highlighted in gray) responsible for the binding with the antigen.

that intermolecular interactions and, hence, viscosity are controllable through modifying specific sites of the antibody.[52] Some works involving experiments and simulations established predictors for viscosity, aggregation, and intermolecular interactions based on amino acid sequences, structural properties, charge distribution, and hydrophobicity of the full sequences and the Fv region of the antibodies.[53−59] By predicting viscosity using artificial neural networks based on experimental and simulation-derived parameters, Schmitt et al. confirmed that sequence-based optimization of mAb properties is a crucial tool for rational drug design.[63] More recently, Armstrong et al. observed that antibody sequence mutations aiming to reduce hydrophobic patches significantly reduced mAb solution viscosity, suggesting the effectiveness of hydrophobic-based predictors; conversely, mutations altering only electrostatic patches were insufficient to influence viscosity.[64] Variable domain mutational analysis identifies Fab−Fab hydrophobic interactions—rather than electrostatic ones—as the major contributors to the high viscosity of an anti-GCGR IgG1.[65] In line with this approach, Li et al. developed a promising tool for controlling mAb aggregation based on systematic pairwise replacement of hydrophobic residues L (leucine), V (valine)/I (isoleucine), and F (phenylalanine) with polar ones, such as Q (glutamine), T (threonine), and Y (tyrosine).[66] Machine learning was also extensively employed to reduce mAb viscosity and predict their developability, always emphasizing the relevance of the Fv domain in the underlying molecular mechanism.[67−69]

Concerning formulation optimization, a widely employed strategy is to improve the formulation by adding molecules able to shield and tune those interactions and to reduce the solution viscosity. So far, some successful excipients have been found among salts (NaCl, Na_2SO_4, NaAc)[70,71] and some amino acids in their pure or salt forms (arginine, glycine,

https://doi.org/10.1021/acs.molpharmaceut.5c00327
Mol. Pharmaceutics 2025, 22, 5373−5388

proline and ornithine, arginine-HCl, histidine-HCl, lysine-HCl).[70,72−75] Other molecules with analogous effects are hydrophobic salts,[76] caffeine,[77] amino acid derivatives,[78] and even amino acid polymers.[79] Moreover, the combination of some viscosity-reducing agents, e.g., amino acids and anionic excipients, has also been observed to enhance the performance of one excipient alone.[80]

1.4. Framework of the Present Study. Despite the progress made in the field, our understanding is still incomplete, and thus the correlation between viscosity, RSA, and cluster formation is still being studied using several techniques including small-angle X-ray and neutron scattering, light scattering, microrheology, viscometry, atomistic and coarse-grained simulations, and colloid theory.[57,81−87]

In the present work, we systematically investigate a set of 9 humanized mAbs produced, characterized, and provided by Lonza AG/Ltd. These mAbs in solution feature big changes in macroscopic viscosity for a given concentration; some of them—mAb12, mAb16, and mAb24—exceed the SC injectability limit (15−20 mPa·s) before high concentrations (see Figure 2 and refs 63,88). However, the most significant differences in their amino acid sequences are in the hypervariable regions of their Fv domains (Figure 1), which confirms that the Fc domain plays a minor role in interprotein interactions[89] compared to the Fv domain.

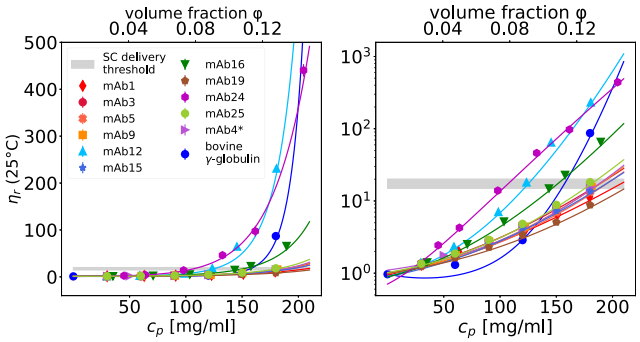

Figure 2. Linear (left) and logarithmic (right) plots showing the relative viscosity $\eta_r = \eta/\eta_0$ (symbols) of aqueous (H_2O) solutions of 10 mAbs of IgG1 subclass and one IgG4 mAb (mAb4*) in 20 mM His-HCl buffer (pH 6.0) at T = 25 °C, versus mAb concentration c_p (lower x-axis) and dry volume fraction φ (upper x-axis). Error bars are mostly hidden behind the symbols. Solid lines are fits to the data using a heuristic model.[88] The gray shaded area stands for the subcutaneous (SC) injectability threshold (∼15 to 20).

In order to systematically explore the link between macroscopic viscosity and microscopic cluster formation, we combined neutron spin-echo (NSE) spectroscopy and small-angle neutron scattering (SANS) experiments, expanding on previous work where we employed neutron backscattering (NBS), SANS, and MD simulations.[88] Several mAbs already investigated in that work show an apparent self-diffusion coefficient D below the value expected for monomers, suggesting the formation of small transient clusters formed by few monomers. NSE was already confirmed as an effective technique to study concentrated mAb solutions,[90−93] revealing the formation of small "reversible clusters with extended open structures"[90] or dimers that can "reversibly associate into loosely connected clusters",[92] likely resulting in higher viscosities.[40,92] NSE allows to investigate several mesoscopic diffusive modes of the proteins at once,[90−94] e.g., translational and rotational components,[94,95] and domain motions. Importantly, due to the longer time scales (up to 200 ns) compared to the previously collected NBS data (≈4 ns), these NSE data close a critical gap in the observation times between the results from viscometry and NBS.

1.5. IgG1 and IgG4 Antibodies. IgG is the most abundant class of immunoglobulins in human blood and is most used in therapeutics. IgG is a Y-shaped ∼150 kDa protein formed by two identical heavy chains (HC) of ∼50 kDa each and two identical light chains (LC) of ∼25 kDa each, cross-linked through interchain disulfide bonds. Both light and heavy chains contain a variable domain (VL, VH) and a constant one (CL, CH); two CH subdomains (CH1, CH2) are linked by a flexible hinge[96,97] that gives IgG a pronounced mobility. In addition, CH_2 and CH_3 subdomains of the heavy chains form the trunk of the Y-structure, which is called the crystallizable fragment (Fc), whereas the two arms of the molecule are formed by CH1, CL, VH, and VL and are called antigen-binding fragments (Fabs). At their extremities, the subdomains VH and VL constitute the variable domain Fv that acts as the actual antigen-binding site. The binding occurs in specific Fv segments, referred as complementarity determining regions (CDRs) or hypervariable regions, which typically exhibit loop structures (Figure 1).

IgGs exist in four different isotypes, IgG1, IgG2, IgG3, and IgG4, which differ in multiple structural and functional details. The present study focuses on IgG1 and IgG4 antibody isotypes. The length of the hinge is of 15 amino acids in IgG1 and 12 in IgG4, leading to the formation of four interchain disulfide bonds in IgG1 and two in IgG4 and resulting in IgG1 being more flexible than IgG4.[98] The hinge stabilization in IgG4 is believed to arise from the amino-acidic substitution Ser228Pro (proline to serine at position 228) from IgG1.[99] The two isotypes also differ in the angles between the Fab regions,[100] in their immune response,[101] viscosity behavior at high concentrations,[102] and self-interactions.[57]

2. MATERIALS AND METHODS

2.1. Sample Preparation. In the present work, we investigate 9 different humanized monoclonal antibodies, 8 IgG1 with κ light chains (mAb3, mAb5, mAb9, mAb19, and mAb25) and λ light chains (mAb12, mAb15, and mAb16) and one IgG4 with κ light chains (mAb4*). Further physicochemical properties of both their full chains and Fv domains are reported in the Supporting Information.

All mAbs were manufactured in-house from Lonza AG/Ltd. Double gene vectors (DGV) containing the heavy and light chains were transfected into CHOK1SV GS-KO cells[103] from Lonza Biologics (Slough, UK) and cultured under selection conditions as stable pooled cultures. Clarified supernatant was obtained by centrifugation followed by filter sterilization using 0.22 μm Stericup Quick Release filters from Merck/MilliporeSigma (Darmstadt, DE). Protein A chromatography was used for mAb purification. All proteins were concentrated to final concentrations of 10−20 mg/mL (nominal), and buffer exchanged into the formulation buffer by tangential flow filtration. A 20 mM histidine-HCl buffer at pH 6.0 was employed as it is done for more than 80% of formulations of approved highly concentrated mAb drug products.[104] All mAb solutions were then frozen in aliquots, stored at −80 °C, and slowly thawed prior to use.

From these solutions, samples for the neutron experiments were prepared by first exchanging the buffer to 20 mM

https://doi.org/10.1021/acs.molpharmaceut.5c00327
Mol. Pharmaceutics 2025, 22, 5373−5388

histidine-HCl in pure D_2O at pD 6.4 (pD = pH + 0.4, so pH = 6.0[105]). To this scope, 15 mL Amicon centrifugal filters with 30 kDa nominal molecular weight cutoff from Merck/MilliporeSigma were employed to obtain a dilution factor of at least 10,000× of the H_2O in the samples. With the same filters, mAb solutions were then concentrated until around 2 mL, in order to reach a concentration of at least 60 mg/mL. The aforementioned deuterated buffer was prepared by dissolving L-histidine monohydrochloride monohydrate (≥98% purity) from Merck/MilliporeSigma in deuterium oxide from Innovachem (Angervilliers, FR) to get a molarity of 20 mM; the desired pH was reached by adjusting with NaOD and the obtained solution was filtered using a 0.22 μm Stericup QuickRelease from Merck/MilliporeSigma. Concentrations of the antibody solutions after buffer exchange were determined by UV−vis via a V-630 Spectrophotometer from Jasco (Tokyo, JP), diluting them 50, 100, 200, 400 and 500×. Samples for neutron experiments were subsequently prepared by diluting concentrated stock solutions until 50 mg/mL. As reference, a polyclonal IgG stock solution was prepared employing lyophilized powder of γ-globulin from bovine serum (≥95% purity, essentially salt-free), purchased from Merck/MilliporeSigma and directly dissolved in a 20 mM histidine-HCl deuterated buffer at pD 6.4. The concentration of the stock solution was measured via UV−vis and the actual sample was prepared by diluting the stock solution to 50 mg/mL (nominal, not further measured). It should be noted that solutions of protiated proteins in D_2O are required in neutron scattering experiments in order to minimize the incoherent contribution of the scattering signal and better distinguish the macromolecules from the solvent.

The selected concentration of 50 mg/mL has been targeted to safely avoid overlapping among the proteins in solution in the neutron spin-echo measurements, based on the following considerations inspired by Girelli et al.[95] Since the distances between the extremal residues of the antibodies are on average shorter than $d_{max} \approx 16$ nm (slightly overestimated, see the Supporting Information), each protein occupies a cubic volume of sidelength d_{max} and therefore can move in a maximum volume $V_{max} \approx 4096$ nm^3 in the solution. Since a sample volume $V_{sample} \sim 2$ mL is needed for the neutron experiments, the maximum number of mAbs in the sample would then be $N_{max} = V_{sample}/V_{max} = (2\text{ mL})/(4096\text{ nm}^3) \sim 4.88 \times 10^{17}$. The overlap protein concentration can be therefore determined as follows

$$c_p^{overlap} = [\text{mAb}]^{overlap} \cdot M_w = \frac{N_{max}}{N_A \cdot V_{sample}} \cdot M_w \quad (1)$$

with N_A being the Avogadro number (6.022×10^{23} mol^{-1}) and M_w the antibody molecular weight (~150 kDa). $[\text{mAb}]^{overlap}$ indicates the overlap mAb molarity calculated as $N_{max}/(N_A \cdot V_{sample})$—number of mAb moles in the sample divided by the sample volume—giving a value of 0.406 mM. The overlap protein concentration $c_p^{overlap}$ is thus ~61 mg/mL, higher than the selected 50 mg/mL. Other approaches to estimate the overlap, e.g., inspired by polymers[106] are possible. In the present case, eq 1 was chosen to obtain a "conservative" lower bound for a possible overlap, ruling out this situation for the studied samples.

2.2. Viscometry and Light Scattering. All of the mAbs were characterized by viscometry, static, and dynamic light scattering (SLS and DLS) as reported by Schmitt et al.[63] and Mosca et al.[88] The measurements were performed at $T = 25$ °C (≃298 K), with concentrations ranging from 180 to 30 mg/mL, in the antibody original formulation buffer (20 mM His-HCl in H_2O, pH 6.0). The instruments used and the measurement protocols are described in refs 63,88.

2.3. Neutron Spin-Echo (NSE) Spectroscopy. Neutron spin-echo (NSE) experiments were conducted on the IN15 spectrometer at the Institut Laue-Langevin (ILL) in Grenoble, France. NSE is a high-resolution inelastic scattering technique that leverages neutron spin precession to measure the velocity changes experienced by neutrons as they interact with matter. This method offers exceptional resolution, allowing to investigate multiscale short-time collective dynamics. Samples were measured at four different instrument configurations, each with a specific incident neutron wavelength and detector angular position (measuring the scattered neutrons): 10 Å−3.5°, 8 Å−5.5°, 6 Å−9.5° and 6 Å−6.5°. The accessible q range spans from 0.028 to 0.19 Å^{-1} for a total of 12 values of the momentum transfer q, resulting from slicing the detector in 3 areas for each configuration. This instrumental setup allows one to explore Fourier times up to 200 ns for the 10 Å−3.5° configuration, up to 100 ns for the 8 Å—5.5° one, and up to 50 ns for the two configurations at 6 Å.

All samples were loaded in flat transparent quartz containers purchased from Aireka Scientific Co., Ltd. (Hong Kong) with the size of 40 × 30 mm^2 and internal thickness of 1 and 2 mm (depending on protein availability), closed with plastic caps, and carefully sealed with Parafilm (Merck/MilliporeSigma) to avoid evaporation of the solutions along the measurements. A graphite sample and the antibody formulation buffer (20 mM His-HCl in D_2O at pD = 6.4) were measured as references for resolution and background, respectively. The sample environment employed was a sample changer with temperature control. All samples were first measured at $T = 37$ °C (≃310 K), temperature of the human body, and afterward at $T = 7$ °C (≃280 K), which is closer to the usual storage temperature of biopharmaceuticals just before administration to patients. A complete acquisition run, accounting for the four aforementioned configurations, was about 4 h for one sample at one temperature. Two samples, selected for their high viscosity, slightly milky appearance, and higher clustering propensity[88]—mAb12 and mAb16—were additionally measured while cooling at just one instrument configuration (6 Å−6.5°) in order to further explore any temperature-driven changes. In this case, echoes were acquired at 4 different temperatures and the whole measurement time was ~1 h. Raw data were resolution-corrected and background-subtracted applying standard data reduction routines in Igor.[107] The analysis was performed by using Python.

2.4. *In Situ* Fixed-Angle Dynamic Light Scattering (DLS) during NSE Measurements. Dynamic light scattering (DLS) measurements at a fixed angle of $\theta = 90°$ were concurrently obtained by using an *in situ* DLS system integrated into the NSE machine. The employed setup is a He−Ne laser with a wavelength of 632.8 nm. Detection was carried out by two Excelitas SPCM AQRH-13 APD detectors, and the correlation function was computed using a Flex02-01 digital correlator in pseudo-cross-correlation mode to mitigate artifacts at short correlation times caused by the detector after pulsing. Unlike standard DLS experiments, in this setup, the autocorrelation functions were averaged over the duration of an NSE scan, which is on average 1 h for each wavelength−

https://doi.org/10.1021/acs.molpharmaceut.5c00327
Mol. Pharmaceutics 2025, 22, 5373−5388

angle combination. As in the NSE experiment, DLS profiles for mAb12 and mAb16 were collected also while cooling.

2.5. Small-Angle Neutron Scattering (SANS). Small-angle neutron scattering (SANS) was performed on the same mAb solutions measured with NSE, in order to determine their time-averaged structural and thermodynamic properties as a function of the temperature and protein type. The SANS experiments were carried out on D22[108] at the ILL. Antibody solutions at nominal concentrations of 50, 20, 10, 5, 2, and 1 mg/mL were prepared, filled into 1 mm plate quartz cuvettes (Hellma, Müllheim, DE), sealed with Parafilm, and placed onto a copper sample holder. Protein concentrations of the samples after dilution were not further measured. A q range from 0.006 to 0.7 Å^{-1} was covered by two detectors (at 16 and 1.7 m from the sample) with respective collimation lengths of 16.5 and 2.5 m. A wavelength of 4.6 Å with a full width at half-maximum (fwhm) wavelength spread of 9% was used. Scattered neutrons were detected using a multitube ^{3}He gas detector with a pixel size of 4 × 8 mm^2. SANS profiles were obtained at set-point temperatures T_{set} of 37 and 22 °C, corresponding to ∼310 and ∼295 K, respectively. For a reduced data set, SANS curves were also measured at 7 °C, corresponding to ∼280 K. The actual temperature of the sample changer rack was monitored throughout the experiment to check how it differed from that of the set-point. For the three temperatures selected ($T_{rack} \pm \Delta T_{rack}$) was calculated, with T_{rack} and ΔT_{rack} being the mean and standard deviation of the values, respectively (Table 1). The largest temperature fluctuations were observed at ∼37 °C, as reported in Table 1. Raw data were saved in NeXuS format[109,110] and data reduction was performed using GRASP, an ILL Matlab-based software.[111] Data were corrected for empty cell scattering, transmission (by measurements performed using beam attenuators), and electronic noise (by measuring a $^{10}B_4C$ absorber). Calibration to absolute scale was performed using attenuated direct beam measurements. The signal of the solvent (20 mM His-HCl deuterated buffer at pD 6.4) at 7 °C was chosen as reference due to its lower incoherent baseline at high q compared to the buffer profiles at 21 and 37 °C and subtracted from sample scattering accounting for the volume occupied by the solvent

Table 1. Differences in the Set-Point and Measured Temperatures of the Sample Changer Rack throughout the SANS Experiment[a]

T_{set} [°C]	$T_{rack} \pm \Delta T_{rack}$ [°C]
37	34.59 ± 1.63
22	21.83 ± 0.21
7	7.21 ± 0.77

[a]The values reported T_{rack} and ΔT_{rack} are, respectively, the mean and standard deviation of the temperatures probed by the rack thermometer during the measurements.

$$I(q)^{sub}_{sample} = I(q)_{sample} - \varphi_{solvent} \cdot I(q)_{solvent} \quad (2)$$

With $\varphi_{protein}$ being the protein volume fraction, the volume occupied by the solvent in the samples is given by

$$\varphi_{solvent} = (1 - \varphi_{protein}) = (1 - c_p \vartheta) \quad (3)$$

where c_p and ϑ are the protein concentration and specific volume, respectively. ϑ was calculated with MDAnalysis[112] using the PDBs of the mAbs and obtaining 0.739 mL/g for mAb3, 0.729 mL/g for mAb5, mAb9, mAb12, mAb15, mAb16, mAb19, mAb25, and 0.727 mL/g for mAb4*.

3. RESULTS AND DISCUSSION

3.1. Viscometry and Light Scattering. As described in refs 63,88, the relative viscosity $\eta_r = \eta/\eta_0$ (with $\eta_0 = \eta_{solvent}$ = 0.92 mPa·s) was analyzed at varying antibody concentration c_p (Figure 2). It must be noted that these viscometry and light scattering results were partially included in the cited works but are reported here for clarity. The data already shown in ref 88 correspond to mAb1, mAb9, mAb12, mAb16, and mAb24, while the additional ones reported here refer to mAb3, mAb5, mAb4*, mAb15, mAb19, and mAb25. The viscosity increase at increasing antibody concentration is strongly mAb-dependent and well-described by the model used in our previous work.[88] From the fit model used, the viscosity values for the samples at 50 mg/mL—the concentration employed in the neutron experiments—were extrapolated (Table 2). From Figure 2, one can observe that all mAbs eventually reach the viscosity limit for syringeability; however, while mAb9, mAb15, mAb25, and mAb4* exhibit high viscosity at ≃180 mg/mL, for some others this is observed already at 140 (mAb16), 120 (mAb12), and 90 mg/mL (mAb24).

Table 2. Relative Viscosities $\eta_r = \eta/\eta_0$ (T = 25°C) at mAb Concentration c_p = 50 mg/mL Calculated from the Model Used to Fit the Data in Figure 2[a]

mAb	η_r (50 mg/mL)	$N_{agg,2}$ (50 mg/mL)
mAb1	1.46 ± 0.14	
mAb3	1.56 ± 0.14	1.51 ± 0.08
mAb5	1.47 ± 0.19	1.26 ± 0.06
mAb9	1.47 ± 0.18	1.48 ± 0.08
mAb4*	1.55 ± 0.37	2.29 ± 0.09
mAb12	1.78 ± 0.46	2.30 ± 0.13
mAb15	1.41 ± 0.06	1.67 ± 0.08
mAb16	1.63 ± 0.14	2.00 ± 0.11
mAb19	1.39 ± 0.26	1.52 ± 0.07
mAb24	2.60 ± 0.24	
mAb25	1.55 ± 0.11	1.47 ± 0.08

[a]Uncertainties associated with the values are calculated by error propagation using the errors on the parameters derived from the fit. The samples characterized by high η_r at high c_p show higher values compared to the others already at 50 mg/mL. The third column reports the average number of monomers per aggregate $N_{agg,2}$ calculated from NSE data at c_p = 50 mg/mL and T = 37°C, assuming a cluster fractal dimension 2. For details, see the text in Section 3.2.

Primary sequence analysis (available in the Supporting Information) reveals that the pI of the Fv domain of mAb4*, mAb12, mAb15, mAb16, and mAb24 is <6.3, identified by Makowski et al. as threshold value below which lay all of the mAbs with high solution viscosity.[68] Fv pI values are in fact 5.44 for mAb4* and mAb12, 5.74 for mAb15, 5.34 for mAb16, and 5.83 for mAb24. Moreover, the Fv net charge for these mAbs with high viscosities is closer to 0 compared to that of the other variants and always slightly negative. One could hypothesize that for these mAbs, the charges on VL and VH regions are essentially equal and opposite, with a slight imbalance on the negative side, in agreement with their opposite correlations with viscosity.[88] These observations again underline the importance of the Fv domain sequence

https://doi.org/10.1021/acs.molpharmaceut.5c00327
Mol. Pharmaceutics 2025, 22, 5373−5388

and confirm its central role in driving intermolecular interactions in the mAbs.[65,89] The differences in viscosity depend on which protein subdomains drive the aggregation and how the oligomers are formed and organized.[52,89] Highest viscosities are apparently determined by a strong presence of Fab-Fc association[48,52] or Fab−Fab interactions.[41,65,82] Both association mechanisms could contribute to high viscosities in mAb24, mAb16, and mAb12 solutions. Fc−Fc association is also likely to be present and is possibly mediated by a small hydrophobic patch at the bottom of the Fc domain (see the Supporting Information). However, since the Fc domain is highly similar in all of the mAbs studied (Figure 1), Fc−Fc cannot explain the increase in viscosity observed in only a few variants (see also Section S5). With regard to light scattering methods, the second virial coefficient A_2 from static light scattering (SLS) and the diffusion-interaction parameter k_D from dynamic light scattering (DLS) can provide insights into the solution behavior of the mAbs by understanding their PPIs, which directly impact their physicochemical stability. These two key parameters obtained by Schmitt et al.[63] are represented here in Figure 3 and their exact values are

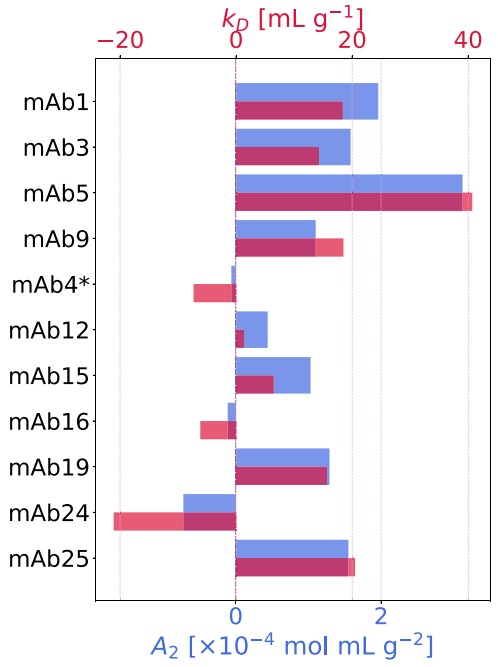

Figure 3. Second virial coefficient A_2 from SLS (lower x-axis) and diffusion-interaction parameter k_D from DLS (upper x-axis) for the mAbs investigated in their original formulation buffer (20 mM His-HCl in H_2O, pH 6.0) at T = 25 °C.

reported in the Supporting Information. A_2 and k_D are generally correlated, with positive values indicating repulsive interactions between mAb molecules and negative values suggesting attractive interactions. Repulsive interactions typically lead to better solution stability, whereas attractive interactions may promote aggregation. Among the mAbs studied, a wide range of behaviors in the selected buffer are observed (Figure 3). mAb5 stands out with the highest positive values for both A_2 and k_D, indicating strong repulsive interactions. This suggests that mAb5 is likely to exhibit excellent solution stability and be less prone to aggregation in the chosen buffer. Similarly, mAb1, mAb3, and mAb25 show moderately positive values, implying good stability characteristics and making them ideal candidates for therapeutic development. Conversely, mAb24 displays the lowest values for both parameters, suggesting strong attractive PPIs, as previously observed.[88] The same trend is observed for mAb4* and mAb16, with slightly weaker mAb−mAb attractions but still pointing toward aggregation and instability. The formulations of these antibodies could be adjusted to improve their stability, e.g., by adding stabilizers or modifying the solution ionic strength. The remaining mAbs exhibit more nuanced behaviors. mAb12 shows a weak positive A_2 but an almost neutral k_D; mAb9, mAb15, and mAb19 show comparable positive A_2, but different positive k_D, higher for mAb9 and lower for mAb15. This suggests that PPIs are less attractive in mAb9 and mAb19 compared to mAb12 and mAb15, but other factors, e.g., microscopic diffusion, should be influencing their behavior and their solution visual appearance. In fact, all of the mAbs whose parameters indicate aggregation are not transparent in solution at 50 mg/mL (see the Supporting Information). More specifically, their k_D values are below the threshold of 20 mL/g set by Kingsbury et al., above which lie all "well-behaved" mAbs in a 10 mM His-HCl buffer at pH 6.0,[113] namely, the ones featuring viscosities < 30 mPa·s and opalescences < 12 nephelometric turbidity units (NTU). This additional constraint on k_D further supports that mAb5, with a $k_D \approx 40$ mL/g, exhibits the most favorable behavior among the studied mAbs. We stress again the fact that these results are strongly buffer-dependent, meaning that some "well-behaved" mAbs in 20 mM His-HCl at pH 6.0 may behave poorly in another formulation.

3.2. Neutron Spin-Echo Spectroscopy. If, as an approximation, internal degrees of freedom are neglected, then antibody solutions can be treated as suspensions of charged colloids. For such systems, different time scales are typically associated with different types of dynamics. Denoting τ_B as the characteristic time of particle momentum autocorrelations and $\tau_I = R_h^2/D_0$ as the characteristic time for diffusion across a distance equal to the particle hydrodynamic radius, the time scale of short-time dynamics is within the range $\tau_B \leq t_{short} \leq \tau_I$.[114] Based on the average size of these proteins, quantified by an average hydrodynamic radius 4 nm $\leq R_h \leq$ 6 nm and a self-diffusion coefficient at the infinitely dilute limit $D_0 \simeq 3.7$ Å^2/ns at 25 °C, the correlation times accessed by the conducted NSE experiment probe the short-time diffusion of the studied mAbs. Specifically, "short" length scales refer to roughly 10 nm, or the size of the protein, and "short" time scales extend up to about 50 ns, which is much smaller than τ_I. The intermediate scattering function (ISF) arising from the measured neutron echo was fitted using a cumulant expansion until the second order of an exponential function, as already done for multidomain proteins[115]

$$\mathrm{ISF} = \frac{I(q,t)}{I(q,0)} = A\cdot\exp\left(k_1 t + \frac{1}{2}k_2 t^2\right) \tag{4}$$

with A, q, and t being a weighing prefactor, the neutron momentum transfer, and the NSE Fourier time, respectively. Echoes measured were fitted independently for each q; an example of an ISF fit (with residuals) is reported in Figure 4. The coefficients k_1 and k_2 in eq 4 represent the first- and second-order cumulants of exponential expansion. The same fit procedure was applied on all of the samples and the fit range employed was the whole Fourier time range allowed by the instrument in the specific configurations used. The first-order

https://doi.org/10.1021/acs.molpharmaceut.5c00327
Mol. Pharmaceutics 2025, 22, 5373−5388

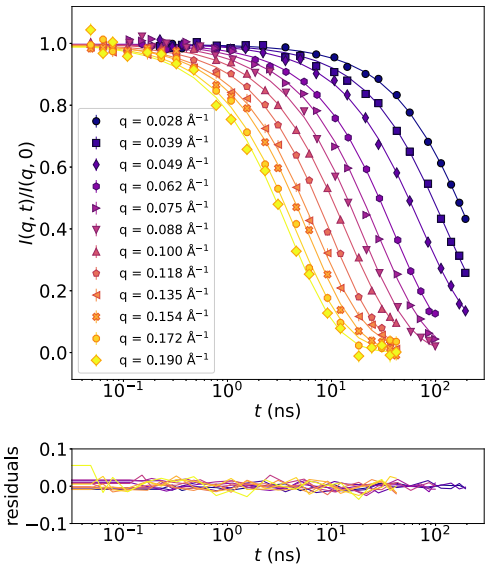

Figure 4. Intermediate scattering function $I(q, t)/I(q, 0)$ (neutron echoes vs Fourier time t) of mAb5 at c_p = 50 mg/mL and T = 37 °C, in solution with 20 mM His-HCl buffer at pD 6.4, measured at the IN15 spectrometer. The experimental points obtained are the combination of the four different instrument configurations used (wavelength of incident neutron and detector angle). Each data series, denoted by a specific symbol and color, corresponds to the neutron echo at a specific value of the momentum transfer q, ranging from 0.028 (dark purple dots) to 0.19 Å^{-1} (yellow diamonds). Error bars are mostly hidden behind the symbols. Solid lines in the corresponding colors are fits to the data with a cumulant expansion of the exponential (eq 4) using all Fourier times. Data are presented on a lin-log scale (top) with their fit residuals at each q depicted with the same color code (bottom).

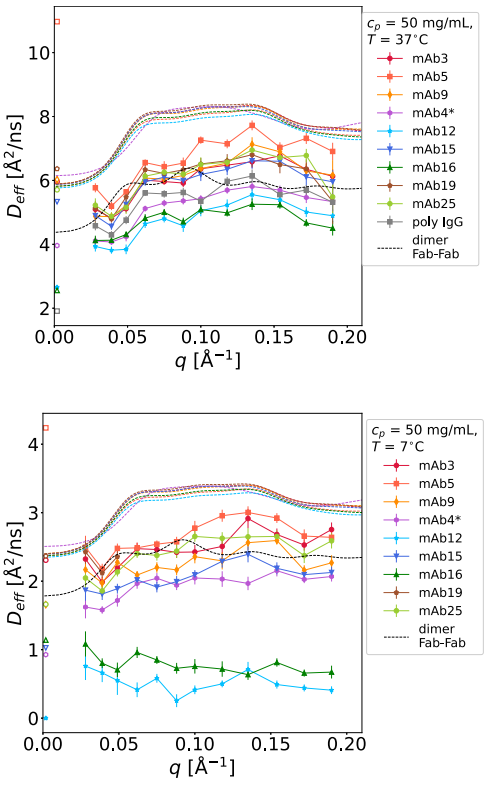

Figure 5. Collective diffusion function of the mAbs. D_{eff} (symbols) for all of the mAbs investigated at c_p = 50 mg/mL, at body temperature T = 37 °C (top) and storage conditions T = 7 °C (bottom), as a function of the momentum transfer q. Solid lines connecting the symbols are guides to the eye, while dashed lines represent the simulated rigid-body diffusion functions of mAb monomers (colored) and dimers (black) calculated from the PDBs of the proteins using Jscatter.[116] The dimer diffusion was determined by using an example Fab−Fab dimer built by merging two mAb5 structures. Open symbols represent D_c^{long} values obtained from DLS data. For further details, see the text.

cumulant k_1 contains insightful information on the diffusion processes in the samples, in fact

$$k_1 = \lim_{t\to 0} \frac{\partial}{\partial t} \frac{I(q, t)}{I(q, 0)} = -\Gamma = -q^2 D_{eff}(q) \tag{5}$$

k_1 is negative by definition and its inverse Γ can be interpreted as the diffusion decay rate with its reciprocal value being the relaxation time τ

$$\tau = \frac{1}{\Gamma} = \frac{1}{q^2 D_{eff}} \tag{6}$$

$D_{eff}(q)$ is the effective short-time diffusion function given by the coherent scattering of the incoming neutrons with the sample, therefore, containing information on its collective dynamics. Figure 5 reports $D_{eff}(q)$ obtained from NSE data for the mAbs in solution at c_p = 50 mg/mL (colored symbols connected by solid lines), at human body and storage temperatures (top and bottom plot, respectively). Dashed colored lines represent the rigid-body diffusion functions of mAb monomers calculated from the PDBs of the proteins using Jscatter.[116] The dashed black line is the diffusion of an example Fab−Fab dimer built by merging two mAb5 structures and again calculated with Jscatter. The choice of mAb5 for this comparison is justified by its remarkably "good behavior" in the selected buffer compared to the others, as discussed in Section 3.1. Since dashed curves are calculated at 20 °C, they were rescaled for temperature and viscosity using the Stokes−Einstein relation and by a factor accounting for the crowding effect at the selected concentration.[117]

A nontrivial q-dependence of the experimental $D_{eff}(q)$ is observed in all samples, also in qualitative agreement with the diffusion curves obtained from the simulations and with previous NSE studies on IgG.[93] The mAbs investigated under the same conditions display diverse diffusive dynamics (Figure 5). For instance, mAb5 shows a faster diffusion compared to mAb12 and mAb16 (Figure 5, top), which are the ones exhibiting higher viscosities already at 50 mg/mL, as reported in Table 2. The shape of their $D_{eff}(q)$ at 7 °C (Figure 5, bottom, cyan, and green symbols) is instead peculiar and to be interpreted with the aid of DLS data simultaneously collected on these two mAbs, which reveal abrupt changes in the correlation functions while cooling to 7 °C; in addition, after the measurements the two samples showed signs of opalescence and phase separation. These observations indicate that the solutions underwent changes during the experiment, resulting in NSE data points collected at different instrument configurations representing varying sample conditions rather than a consistent state. The peculiar behavior of the diffusion curve is therefore signature of phase separation.[46] Further details are given in the Supporting Information. In Figure 5, the experimentally derived $D_{eff}(q)$ is compared to the one calculated via MD simulations using the PDB structures of the

https://doi.org/10.1021/acs.molpharmaceut.5c00327
Mol. Pharmaceutics 2025, 22, 5373−5388

mAbs and considering them as rigid bodies. These calculated diffusion functions are shown as colored dashed lines in Figure 5 for monomeric structures, while an example of a dimer diffusion is depicted as a black dashed line. In this case, the dimer structure was built by manually combining two mAb5 monomers via their Fab arms. The comparison between the experimental and computed diffusion of the mAbs provides insights on their clustering behavior. Figure 5 shows that all of the experimental diffusion functions lie under the prediction for their corresponding monomeric structure, indicating oligomerization already at 50 mg/mL at 37 °C, which becomes more marked at 7 °C. For most of the mAbs, $D_{\mathrm{eff}}(q)$ lies between the monomeric and dimeric diffusion predictions, consistent with NBS results from our previous work.[88] The mAbs exhibiting higher viscosity lie instead under the dimer line as already observed,[88] suggesting the presence of attractive intermolecular interactions.[44,118] This can lead to the formation of short-lived clusters of more than two mAb monomers in these samples, e.g., trimers or small network-like assemblies, which have been previously identified as the cause of opalescence and high viscosity in mAb solutions.[48,49,119] Since the clusters do not reach sizes larger than dimers for "well-behaved mAbs" and small oligomers for the stickiest ones, the aggregation mechanism might be nucleation-dominated (ND).[89] In order to approximately determine the number of monomers per cluster for every mAb, an average aggregation number N_{agg} was calculated assuming a cluster fractal dimension $d_f = 3$ as follows: $N_{\mathrm{agg},3} = M_w^{\mathrm{eff}}/M_w^{\mathrm{sim}} \sim (R_h^{\mathrm{eff}}/R_h^{\mathrm{sim}})^3$, where M_w^{exp} and M_w^{sim} are the molecular weight of an experimentally observed aggregate and of a simulated mAb monomer, respectively, both proportional to the third power of their hydrodynamic radii R_h^{eff} and R_h^{sim}. According to the Stokes−Einstein relation, $R_h \sim 1/D(q \to 0)$; therefore, $N_{\mathrm{agg},3} \sim [D_{\mathrm{eff}}(q \to 0)/D_{\mathrm{sim}}(q \to 0)]^3$, where $D_{\mathrm{sim}}(q \to 0)$ is the NSE diffusion coefficient at the lowest q measured (0.028 Å^{-1}, corresponding to the first experimental point in the diffusion functions in Figure 5). However, a value of $d_f \sim 2$ emerging from SANS data (see Figure S12) suggests that the aggregates are not fully compact, so a better estimate for N_{agg} could be $N_{\mathrm{agg},2} \sim (R_h^{\mathrm{eff}}/R_h^{\mathrm{sim}})^2 \sim [D_{\mathrm{eff}}(q \to 0)/D_{\mathrm{sim}}(q \to 0)]^2$. At physiological temperature, $N_{\mathrm{agg},2} \lesssim 1.7$ for the antibodies with a good viscosity behavior (mAb3, mAb5, mAb9, mAb15, mAb19, mAb25, and polyclonal IgG), while $2 \lesssim N_{\mathrm{agg},2} < 2.5$ for mAb12, mAb16, and mAb4*. After cooling to 7 °C, no significant changes are observed for most of the mAbs, except for mAb15 (with $N_{\mathrm{agg},2}$ increasing from 1.7 to 1.8) and mAb4* (from 2.3 to 2.4). We did not evaluate N_{agg} for mAb12 and mAb16 because the solutions appeared either milky and turbid or phase-separated at 7 °C. Furthermore, it is of great interest to link N_{agg} evaluated using both NSE experimental data and simulated diffusion with the relative mAb solution viscosity η_r at 50 mg/mL and 25 °C (Table 2). For IgG1 mAbs, an increase in N_{agg} corresponds to a higher solution viscosity, whereas for mAb4*, the only IgG4 in the set, a moderate propensity to aggregation is not associated with high solution viscosity. Differences in the relation between viscosity and cluster size among antibody subclasses have been reported earlier and were attributed to subclass-specific "interaction hot spots".[120] One could hypothesize that mAb4* forms less extended clusters due to its intrinsic rigidity compared with the other IgG1 mAbs. The change in N_{agg} upon temperature variation for all of the samples is reported in the Supporting Information, along with η_r (25 °C) trend *vs* N_{agg} (for both d_f = 2, 3).

Figure 5 also shows how cooling to 7 °C slows all of the dynamical components, from the translations at low q to the internal relaxations at higher q, by smoothing the $D_{\mathrm{eff}}(q)$. The drop in temperature also strengthens the PPIs, binding, for example, Fab from one mAb and Fc from another, thus altering the internal dynamics of individual proteins.[121] Also note that the purple curve representing mAb4* (the only IgG4 in the set) appears to be smoother than the others depicting the rest of the mAbs investigated (all IgG1), consistent with the well-known reduced flexibility of the IgG4 variant compared to IgG1.[98]

Since at finite concentrations intermolecular interactions cannot be neglected, $D_{\mathrm{eff}}(q)$ contains information about the sample solution structure and its hydrodynamic interaction and can be expressed as[117]

$$D_{\mathrm{eff}}(q) = D_0 \frac{H(q)}{S(q)} \tag{7}$$

with $S(q)$ and $H(q)$ being the structure factor obtained from SANS and the hydrodynamic function, respectively. At infinite dilution, there are no hydrodynamic interactions; therefore, $H(q) = 1$. At nonzero particle concentration, the hydrodynamic interactions give rise to undulations in $H(q)$.[114] Furthermore, the coefficient of the second-order term in the fit function used (eq 4), that is k_2, can be linked to the polydispersity of the samples via the following relation borrowed from light scattering theory[122,123]

$$\mathrm{PDI} = \frac{k_2}{k_1^2} \tag{8}$$

The polydispersity index (PDI) trend *vs* q from NSE fits is reported in Figure S2. Overall, mAb solutions with lower viscosity are characterized by mild polydispersity, while mAb12 and mAb16 are characterized by a moderate one. MAb4* solution is also quite polydisperse despite its viscosity being below the threshold for SC injectability. Furthermore, polydispersity increases upon cooling from 37 to 7 °C and the shape of PDI(q) becomes less smooth for all of the mAbs, especially for mAb15, mAb4*, and mAb25.

3.2.1. Fixed-Angle Dynamic Light Scattering. DLS data at a fixed angle were collected in order to monitor sample stability over time while conducting the NSE experiment. For the samples showing a basically constant decay over time, namely, all of the solutions at 37 °C, the correlation functions $g_2(t)$ obtained were fitted with a single exponential indicating one relaxation process

$$g_2(t) = A(1 + B\mathrm{e}^{-2\Gamma t}) \tag{9}$$

with A and B being the baseline and the intercept of the correlation function, respectively, and

$$\Gamma = D_c^{\mathrm{long}} q^2 \tag{10}$$

where D_c^{long} is the long-time collective diffusion coefficient, as opposed to the short-time one obtained from NSE. The momentum transfer q probed reads

$$q = \frac{4\pi n}{\lambda_0} \sin\frac{\theta}{2} \tag{11}$$

https://doi.org/10.1021/acs.molpharmaceut.5c00327
Mol. Pharmaceutics 2025, 22, 5373−5388

where λ_0 = 632.8 nm is the laser wavelength, θ = 90° is the fixed angle where the scattered light is detected, and $n = n(\lambda_0, T)$ is the refractive index of D_2O calculated at the temperatures of interest via interpolation from existing data fitted with the Cauchy formula as in ref 124. The values obtained are 1.33 and 1.32 at 7 and 37 °C, respectively. The momentum transfer probed by the DLS measurements performed is therefore 0.0186 $Å^{-1}$, as calculated from eq 11, corresponding to a real-space distance of 33.8 nm, much larger than the hydrodynamic radius of an antibody monomer. This approach was also applied to the samples at 7 °C, along with a double-exponential fit for the ones exhibiting an additional shoulder and a more turbid visual appearance, e.g., the stickiest and most viscous ones (mAb12 and mAb16). DLS was a very useful diagnostic tool for assessing solution stability during the NSE investigation, revealing phase separation and helping in data interpretation. From the single-exponential fits, the long-time collective diffusion coefficient D_c^{long} and the hydrodynamic radius R_h of the samples were extracted, the latter calculated based on the Stokes−Einstein relation. All correlation functions obtained from DLS, D_c^{long} and R_h trends over temperature, some additional information on this analysis, some pictures of the samples taken after the experiment, and a more detailed discussion are reported in Sections S1.1 and S2. DLS can also access the polydispersity index (PDI) in mAb solutions, which can be systematically studied upon crowding and related to viscosity.[81] However, due to the setup used and samples being at a fixed concentration, systematic information regarding the PDI is limited for our samples (Figure S9).

3.2.2. Normal Modes (NM) of the Antibodies. The simulated diffusion function $D_{sim}(q)$ of different mAbs was calculated via Jscatter[116] using the PDB files of the proteins as inputs. $D_{sim}(q)$ was first evaluated by solely taking into account the first 6 trivial eigenmodes (3 translational + 3 rotational degrees of freedom), thus treating the antibodies as rigid proteins with their shape and anisotropy. Subsequently, $D_{sim}(q)$ was calculated progressively by adding the contributions of higher-order vibrational normal modes (NM). Figure 6 reports $D_{sim}(q)$ for the mAb monomeric structures and for an example dimeric one only taking into account translations and rotations (top plot), and also accounting for additional NM—other plots, NM 7, 8, 9, 10, 11, 12. From previous NSE studies, it is known that the antibody flexible hinge region acts as an entropic spring, around which the three fragments (Fc and 2 Fabs) move with Brownian motion in a harmonic potential.[93] The observable diffusive motion of the antibodies should thus be seen as a combination of these harmonic NM. The NM effective diffusion curves do not show remarkable differences among all of the IgG1 monomeric mAbs (Figure 6). However, mAb12, mAb15, and mAb16 reach higher peak values in the diffusion calculation that includes NM 7, 8, 9, and 11, suggesting more flexible structures able to explore more extended modes that may enhance self-association and, hence, explain their high viscosity.

Major discrepancies are instead observed between IgG1 and IgG4 proteins, with the latter systematically displaying a different as well as a smoother shape of the diffusion function and significantly lower values, especially when additional NM values are considered, with respect to the IgG1 isotype. This again points toward a higher rigidity and thus lower propensity to wide movements of IgG4 with respect to IgG1 molecules,[98] as already observed in the $D_{eff}(q)$ obtained from NSE data. In this regard, one might be tempted to fit the experimental

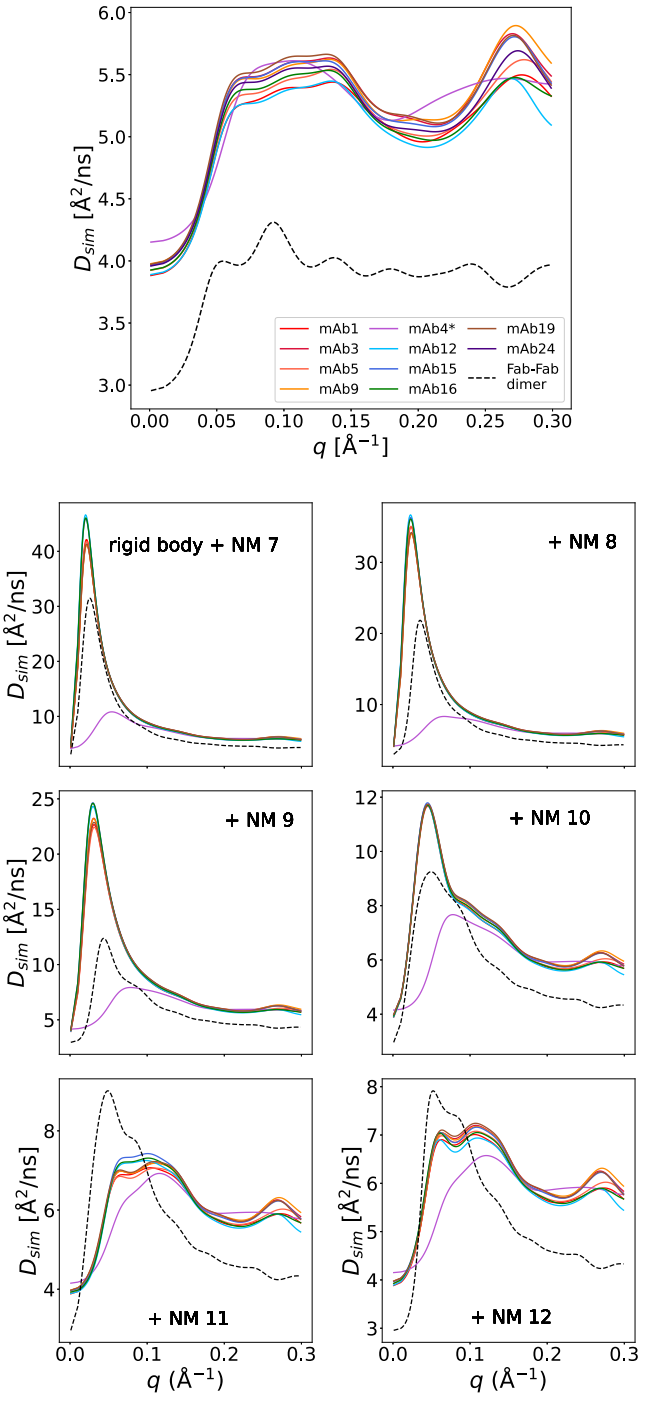

Figure 6. Simulated effective diffusion D_{sim} of different mAb monomeric structures (colored solid lines) and one example Fab−Fab dimeric structure built using mAb5 monomers (black dashed line) calculated via Jscatter,[116] by considering the proteins as rigid bodies, therefore, only taking into account 3 translational + 3 rotational degrees of freedom (top plot), and by evaluating relaxations arising from additional normal modes (NM) (other plots, NM 7, 8, 9, 10, 11, and 12).

$D_{eff}(q)$ by using a linear combination of the simulated diffusion curves. However, due to the hypothesized transient cluster formation, $D_{eff}(q)$ contains heterogeneous information, and a quantitative normal-mode analysis based on rigid dimer or trimer structures would not represent the physics on the

https://doi.org/10.1021/acs.molpharmaceut.5c00327
Mol. Pharmaceutics 2025, 22, 5373−5388

systems. Therefore, our discussion must remain limited to the deviation from monomer D_{sim} and to the calculation of N_{agg}.

3.3. Small-Angle Neutron Scattering. In addition to providing structural information on the nanometer-to-micrometer scale of mAb solutions, SANS also sheds light on their intermolecular interactions. The intensity of scattered neutrons measured with SANS is expressed as[125,126]

$$I(q) = n(\Delta\rho_{SL})^2 V_{part}^2 P(q) S(q) \tag{12}$$

with n being the particle number density, $\Delta\rho_{SL}$ the difference in scattering length density between the solvent and the sample particles (also known as the scattering contrast), and V_{part} being the volume of a single particle.[125,126] $P(q)$ is the particle form factor, determined by the protein shape,[126,127] which equals unity in the $q \to 0$ limit. $S(q)$ is the structure factor,[128−130] which contains the information on the mutual interactions between mAbs and their organization in solution and $S(q) = 1$ for $c_p \to 0$, when PPIs are negligible. From eq 12, data were fitted via Python-written routines employing a triaxial ellipsoid $P(q)$ and a sticky hard sphere $S(q)$. The ellipsoid radii obtained from the fits are globally consistent upon concentration, temperature, and mAb variant below 20 mg/mL, and their values are in the following ranges, consistent with previous works:[131] 100−110 Å for R_a, 37−40 Å for R_b, and 20−24 Å for R_c. At increasing concentration and decreasing temperature, an increase in R_a is observed for the mAbs with significant aggregation propensity (mAb4*, mAb12, and mAb16) with values reaching ∼200 Å. For mAbs less prone to aggregation, like mAb3 and mAb5, R_a is instead in the range 75−95 Å. Some fit examples for SANS data are shown in the Supporting Information. Given a minimum accessible q of 0.006 Å^{-1} in the SANS experiment conducted, the largest length scale that can be resolved corresponds to R_{max} = 104.7 nm (= $2\pi/q_{min}$) in real space. Considering an average antibody radius R being in the range $4 \le R \le 6$ nm, the q-region satisfying the criteria $qR < 1.3$ required for the Guinier approximation is $0.10 \le q \le 0.16$ Å^{-1}. Mathematically, the Guinier approximation for the scattering intensity reads

$$\ln I(q) = \ln I(0) - \frac{R_g^2}{3} q^2 \tag{13}$$

where $I(0)$ is the intensity at zero scattering angle and R_g is the radius of gyration of the particles.

In Figure 7, we report the curves for different mAbs at the same concentration of 20 mg/mL at T = 37 °C (top) and T = 21 °C (bottom). SANS profiles for the samples at other concentrations and mAb9 data at T = 7 °C are reported in the Supporting Information. An example of a concentration series measured for mAb4* (Figure 8) shows a decreasing intensity at low q and decreasing protein concentration, which is indeed expected for these systems. Large error bars at $q \approx 0.04$ Å^{-1} arise from stitching together data from two detectors, with this specific q being the overlap point. Moreover, a slight intensity decrease at the lowest q is observed for 2, 5, and 10 mg/mL (Figure 8). Due to the lower amount of material present in solution upon dilution, the signal-to-noise ratio decreases and so does the intensity. For the same reason, at these concentrations, it is more likely to have buffer subtraction issues.

At first glance, one can already hypothesize about the nature and intensity of PPIs. In particular, mAb16 and mAb12 (cyan and green curves in Figure 7) display high values of $I(q \to 0)$,

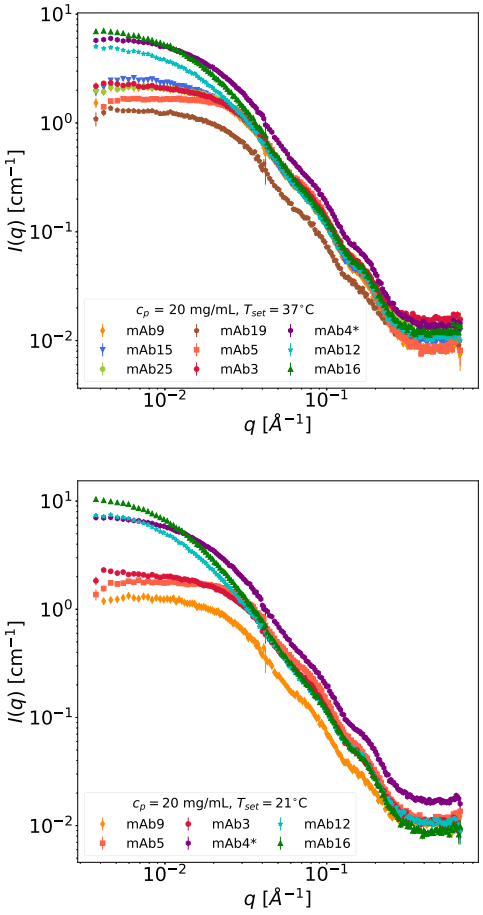

Figure 7. SANS profiles of all mAbs at c_p = 20 mg/mL at T = 37 °C (top) and T = 21 °C (bottom), background-subtracted taking into account the volume fraction occupied by the solvent.

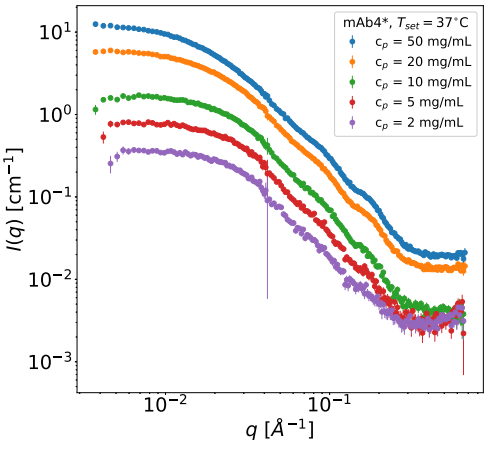

Figure 8. SANS profiles of mAb4* (IgG4) at T = 37 °C at different protein concentrations c_p ranging from 50 to 2 mg/mL, background-subtracted taking into account the volume fraction occupied by the solvent.

clearly suggesting the presence of more attractive PPIs already at 20 mg/mL. mAb5 (coral square curve) shows, on the other hand, lower intensity at low q, indicating the presence of more repulsive interactions. The effect of temperature variation on the curves is more subtle. These qualitative considerations are also confirmed by a quantitative Guinier analysis performed on all samples by using eq 13. We note that the Guinier analysis

https://doi.org/10.1021/acs.molpharmaceut.5c00327
Mol. Pharmaceutics 2025, 22, 5373−5388

was also performed on the samples with non-negligible $S(q)$ effects, so the radius of gyration obtained is an apparent one and will be denoted with R_g^{app}. Despite this, detecting changes in R_g^{app} is, anyway, very informative for potential oligomerization. An increase in R_g^{app} is observed at the following conditions: (i) at increasing c_p for every mAb individually, due to crowding effect; (ii) for the mAb variants exhibiting higher solution viscosities at the same c_p; and (iii) at decreasing temperature. Guinier plots with fit results for all of the samples are reported in the Supporting Information, along with R_g^{app} trends over mAb concentration and temperature. Regarding mAb4*, despite its clustering propensity inferred from NSE, it displays a lower apparent R_g^{app} compared to the most viscous IgG1 mAbs (mA12 and mA16). Its higher molecular rigidity—extensively documented in literature[98] and also visible in its SANS curves with quite sharp peaks in Kratky representation (see the Supporting Information)—causes it to explore fewer conformations and form less extended aggregates than mAb12 and mAb16, which may instead form assemblies with "inefficient packing".[120]

4. CONCLUSIONS

In this work, we present a systematic comparison of an unprecedented series of monoclonal antibodies (mAbs)—8 IgG1 and 1 IgG4—evaluating various physicochemical properties, such as macroscopic viscosity, multiscale diffusion, protein−protein interactions (PPIs), and molecular flexibility. This study builds on previous findings that observed the formation of transient, small clusters in mAb solutions, which dissociate at physiological temperatures.[88] Via NSE, we investigate the collective diffusion of the mAbs in the q-region from 0.03 to 0.19 Å^{-1}, corresponding to a longer length scale than the one previously probed by NBS,[88] and to longer coherence times. We observe that all of the mAbs undergo self-association in the time window explored. These transient clusters are composed of dimers, trimers, and network-like assemblies associating in a nucleation-dominated (ND) mechanism,[89] often leading to solution opalesce and even phase separation. In the present work, *in situ* fixed-angle DLS was used as an essential diagnostic tool in order to monitor the solution stability over time and temperature variation during NSE measurement. Notably, we observe the formation of transient clusters at concentrations of 50 mg/mL, which is below the concentrations typically required for pharmaceutical formulations to be administered via subcutaneous injection. As observed in previous works, studying protein solutions at semidilute conditions could still help in the understanding of their behavior at high concentrations.[47,52,132,133] This raises important considerations for formulation development.

Additionally, we compare our NSE experimental results with the simulated diffusion calculated from the PDB files of all of the antibodies, and we find qualitative agreement between the two. Through this comparison, we also confirm the hypothesis of small clusters formed by few monomers by estimating the number of monomers per aggregate, and we relate it to the solution viscosity. Moreover, both NSE data and normal-mode (NM) analysis highlight differences in the microscopic dynamics of IgG1 and IgG4 antibodies, particularly in terms of their molecular flexibility, which appears to favor the first over the latter.

SANS measurements were also carried out to assess the nature and intensity of intermolecular interactions, revealing a higher aggregation propensity in solutions for the mAbs with the highest macroscopic viscosities, which becomes more important at a decreasing temperature. Remarkable differences between the IgG4 mAb and all of the other IgG1 variants are revealed by SANS too. Aided by all of the techniques employed in this work, we can hypothesize that the more pronounced rigidity of the IgG4 mAb studied here limits its ability to explore different conformations and influences its cluster formation. In fact, despite its moderate aggregation propensity, its solution viscosity still remains below the SC injectability threshold even at high concentrations, meaning that it can form less extended assemblies with a more efficient packing.

In conclusion, key factors typically influencing the behavior of mAbs in solution include surface charge and hydrophobicity, which play crucial roles in determining both molecular interactions and aggregation tendencies. In the present case, we hypothesize that hydrophobic interactions can drive Fc−Fc association in all variants but electrostatic Fab−Fab interactions play a major role in leading to high viscosities.

These insights provide a deeper understanding of the physical properties of mAb solutions in general, offering valuable guidance for optimizing therapeutic antibody formulations and further corroborate the efficacy of neutron scattering techniques for pharmaceutical applications.

■ ASSOCIATED CONTENT

Data Availability Statement

Neutron data are permanently curated under DOI and are available in ref 134, in agreement with ILL data policy.

Supporting Information

The Supporting Information is available free of charge at https://pubs.acs.org/doi/10.1021/acs.molpharmaceut.5c00327.

Additional information on NSE data analysis, NSE measurements while cooling, visual appearance of the samples after the experiment, DLS results, additional SANS data, Guinier and Kratky plots of SANS data, combination of NSE, SANS, and DLS, physicochemical properties of the antibodies (full sequence and Fv domains), and distribution of charged and hydrophobic residues (PDF)

■ AUTHOR INFORMATION

Corresponding Authors

Ilaria Mosca − *Institut für Angewandte Physik, Universität Tübingen, 72076 Tübingen, Germany; Institut Max von Laue-Paul Langevin, 38042 Grenoble, France;* Present Address: Dipartimento di Fisica e Geologia, Università degli Studi di Perugia, Via Alessandro Pascoli, 06123 Perugia, Italy; orcid.org/0000-0001-9211-5697; Email: ilaria.mosca@unipg.it

Frank Schreiber − *Institut für Angewandte Physik, Universität Tübingen, 72076 Tübingen, Germany; Institut Max von Laue-Paul Langevin, 38042 Grenoble, France;* orcid.org/0000-0003-3659-6718; Email: seydel@ill.eu

Tilo Seydel − *Institut Max von Laue-Paul Langevin, 38042 Grenoble, France;* orcid.org/0000-0001-9630-1630; Email: frank.schreiber@uni-tuebingen.de

Authors

Christian Beck − *Institut für Angewandte Physik, Universität Tübingen, 72076 Tübingen, Germany; Institut Max von*

https://doi.org/10.1021/acs.molpharmaceut.5c00327
Mol. Pharmaceutics 2025, 22, 5373−5388

Laue-Paul Langevin, 38042 Grenoble, France; orcid.org/0000-0001-7214-3447

Laura Mateo-Miñarro − *Institut für Angewandte Physik, Universität Tübingen, 72076 Tübingen, Germany; Institut Max von Laue-Paul Langevin, 38042 Grenoble, France; Université Grenoble-Alpes, 38400 Saint-Martin d'Hères, France*

Roody Nasro − *Institut für Angewandte Physik, Universität Tübingen, 72076 Tübingen, Germany*

Anna Carlotta Grundel − *Institut Max von Laue-Paul Langevin, 38042 Grenoble, France; Fakultät für Physik und Astronomie, Universität Heidelberg, 69120 Heidelberg, Germany*

Ingo Hoffmann − *Institut Max von Laue-Paul Langevin, 38042 Grenoble, France;* orcid.org/0000-0001-7178-6467

Kévin Pounot − *European Synchrotron Radiation Facility, 38042 Grenoble, France*

Olga Matsarskaia − *Institut Max von Laue-Paul Langevin, 38042 Grenoble, France;* orcid.org/0000-0002-7293-7287

Christoph Grapentin − *Lonza AG/Ltd., 4057 Basel, Switzerland*

Complete contact information is available at: https://pubs.acs.org/10.1021/acs.molpharmaceut.5c00327

Author Contributions

All authors performed experiments, contributed to data analysis, and in the writing of the manuscript. I.M. wrote the manuscript first draft. I.M., C.B., L.M.-M., R.N., and A.C.G. prepared the samples. F.S., T.S., O.M., and C.G. designed the research and are coproposers and supervisors of the associated InnovaXN Project (innovaxn.eu).

Notes

The authors declare no competing financial interest.

■ ACKNOWLEDGMENTS

This research has been supported by InnovaXN, a EU Horizon 2020 MSCA COFUND Programme (innovaxn.eu, Grant Agreement No. 847439). I.M. acknowledges an ILL Ph.D. studentship funded by this programme. The authors are grateful for support by the DFG and ANR (ANR-21-CE06-0047 IDPXN, ANR-16-CE92-0009, ImmunoglobulinCrowding), in the initial phase of this project, and by the BMBF (ErUM-pro 05K19VTB and 05K22VTA). The authors acknowledge the support of the ESRF and ILL Partnership for Soft Condensed Matter (PSCM) for providing access to equipment and lab facilities. The authors are also thankful to Juliette Devos (Life Science group at ILL, Grenoble) for support, Jonathan Schmitt (Lonza Basel) for advice and help with viscometry, Laura Stingaciu (ORNL) for stimulating discussions, and Ralf Biehl (JCNS) for advice on the Jscatter software.

■ REFERENCES

(1) Köhler, G.; Milstein, C. Continuous cultures of fused cells secreting antibody of predefined specificity. *Nature* **1975**, *256*, 495−497.

(2) Ecker, D. M.; Jones, S. D.; Levine, H. L. The therapeutic monoclonal antibody market. *mAbs* **2015**, *7* (1), 9−14.

(3) Kaplon, H.; Crescioli, S.; Chenoweth, A.; Visweswaraiah, J.; Reichert, J. M. Antibodies to watch in 2023. *mAbs* **2023**, *15*, No. 2153410.

(4) De la Torre, B. G.; Albericio, F. The pharmaceutical industry in 2023: an analysis of FDA drug approvals from the perspective of molecules. *Molecules* **2024**, *29*, 585.

(5) Crescioli, S.; Kaplon, H.; Chenoweth, A.; Wang, L.; Visweswaraiah, J.; Reichert, J. M. Antibodies to watch in 2024. *mAbs* **2024**, *16* (1), No. 2297450.

(6) Crescioli, S.; Kaplon, H.; Wang, L.; Visweswaraiah, J.; Kapoor, V.; Reichert, J. M. Antibodies to watch in 2025. *mAbs* **2025**, *17* (1), No. 2443538.

(7) Scott, A. M.; Allison, J. P.; Wolchok, J. D. Monoclonal antibodies in cancer therapy. *Cancer Immun.* **2012**, *12* (1), No. 14.

(8) Saini, S.; Gulati, N.; Awasthi, R.; Arora, V.; Singh, S. K.; Kumar, S.; Gupta, G.; Dua, K.; Pahwa, R.; Dureja, H. Monoclonal antibodies and antibody-drug conjugates as emerging therapeutics for breast cancer treatment. *Curr. Drug Delivery* **2024**, *21* (7), 993−1009, DOI: 10.2174/1567201820666230731094258.

(9) Das, R. T. Cell receptor-engaging monoclonal antibodies mobilize the anti-tumor functions of invariant Natural Killer T Cells. *Crit. Rev. Oncog.* **2024**, *29* (1), 69−81.

(10) Flego, M.; Ascione, A.; Cianfriglia, M.; Vella, S. Clinical development of monoclonal antibody-based drugs in HIV and HCV diseases. *BMC Med.* **2013**, *11*, No. 4.

(11) Bruno, V.; Battaglia, G.; Nicoletti, F. The advent of monoclonal antibodies in the treatment of chronic autoimmune diseases. *Neurol. Sci.* **2011**, *31*, 283−288.

(12) Voge, N. V.; Alvarez, E. Monoclonal antibodies in multiple sclerosis: Present and future. *Biomedicines* **2019**, *7*, 20.

(13) Pour-Reza-Gholi, F.; Assadiasl, S. Eculizumab in kidney diseases. *J. Nephropharmacol.* **2024**, *13* (1), No. e10630.

(14) Raffaelli, B.; Neeb, L.; Reuter, U. Monoclonal antibodies for the prevention of migraine. *Expert Opin. Biol. Ther.* **2019**, *19*, 1307−1317.

(15) Mínguez-Olaondo, A.; López-Bravo, A.; Quintas, S.; Nieves-Castellanos, C.; Layos-Romero, A.; Belvís, R.; Irimia, P.; Díaz-Insa, S. New therapeutic era for migraine attacks with recently approved monoclonal antibodies, ditans and gepants. *Rev. Neurol.* **2024**, *78*, 47−57.

(16) Kayentao, K.; Ongoiba, A.; Preston, A. C.; Healy, S. A.; Hu, Z.; Skinner, J.; Doumbo, S.; Wang, J.; Cisse, H.; Doumtabe, D.; et al. Subcutaneous administration of a monoclonal antibody to prevent malaria. *N. Engl. J. Med.* **2024**, *390*, 1549−1559.

(17) Van Dyck, C. H. Anti-amyloid-β monoclonal antibodies for Alzheimer's disease: pitfalls and promise. *Biol. Psychiatry* **2018**, *83*, 311−319.

(18) Lacorte, E.; Ancidoni, A.; Zaccaria, V.; Remoli, G.; Tariciotti, L.; Bellomo, G.; Sciancalepore, F.; Corbo, M.; Lombardo, F. L.; Bacigalupo, I.; et al. Safety and efficacy of monoclonal antibodies for Alzheimer's disease: a systematic review and meta-analysis of published and unpublished clinical trials. *J. Alzheimers Dis.* **2022**, *87*, 101−129.

(19) Perneczky, R.; Dom, G.; Chan, A.; Falkai, P.; Bassetti, C. Anti-amyloid antibody treatments for Alzheimer's disease. *Eur. J. Neurol.* **2024**, *31*, No. e16049.

(20) Cummings, J.; Osse, A. M. L.; Cammann, D.; Powell, J.; Chen, J. Anti-amyloid monoclonal antibodies for the treatment of Alzheimer's disease. *BioDrugs* **2024**, *38*, 5−22.

(21) Ebell, M. H.; Barry, H. C.; Baduni, K.; Grasso, G. Clinically important benefits and harms of monoclonal antibodies targeting amyloid for the treatment of Alzheimer's disease: A systematic review and meta-analysis. *Ann. Fam Med.* **2024**, *22*, 50−62.

(22) Digma, L. A.; Winer, J. R.; Greicius, M. D. Substantial doubt remains about the efficacy of anti-amyloid antibodies. *J. Alzheimers Dis.* **2024**, *97*, 567−572.

(23) Tashima, T. Delivery of orally administered digestible antibodies using nanoparticles. *Int. J. Mol. Sci.* **2021**, *22*, 3349.

(24) Viola, M.; Sequeira, J.; Seiça, R.; Veiga, F.; Serra, J.; Santos, A. C.; Ribeiro, A. J. Subcutaneous delivery of monoclonal antibodies: how do we get there? *J. Controlled Release* **2018**, *286*, 301−314.

(25) Zhong, X.; Liu, Y.; Ardekani, A. M. A compartment model for subcutaneous injection of monoclonal antibodies. *Int. J. Pharm.* **2024**, *650*, No. 123687.
(26) Stoner, K. L.; Harder, H.; Fallowfield, L. J.; Jenkins, V. A. Intravenous versus subcutaneous drug administration. Which do patients prefer? A systematic review. *Patient* **2015**, *8*, 145−153.
(27) Hilley, P.; Wong, D.; Ma, R.; Peterson, A.; De Cruz, P. Transitioning patients from intravenous to subcutaneous infliximab and vedolizumab for inflammatory bowel disease: what is the opportunity cost of improving access to healthcare. *Intern. Med. J.* **2024**, *54*, 970−979, DOI: 10.1111/imj.16311.
(28) Napolitano, D.; Settanni, C. R.; Parisio, L.; Orgiana, N.; Poscia, A.; Schiavoni, E.; Turchini, L.; Cascio, A. L.; Germini, F.; Sblendorio, E.; et al. Transition from intravenous to subcutaneous biological therapies in inflammatory bowel disease: An online survey of patients. *Indian J. Gastroenterol.* **2024**, *43*, 215−225.
(29) Berteau, C.; Filipe-Santos, O.; Wang, T.; Rojas, H. E.; Granger, C.; Schwarzenbach, F. Evaluation of the impact of viscosity, injection volume, and injection flow rate on subcutaneous injection tolerance. *Med. Devices: Evidence Res.* **2015**, *8*, 473.
(30) Deokar, V.; Sharma, A.; Mody, R.; Volety, S. M. Comparison of strategies in development and manufacturing of low viscosity, ultra-high concentration formulation for IgG1 antibody. *J. Pharm. Sci.* **2020**, *109*, 3579−3589.
(31) Shire, S. J.; Shahrokh, Z.; Liu, J. Challenges in the development of high protein concentration formulations. *J. Pharm. Sci.* **2004**, *93*, 1390−1402.
(32) Garidel, P.; Kuhn, A. B.; Schäfer, L. V.; Karow-Zwick, A. R.; Blech, M. High-concentration protein formulations: how high is high? *Eur. J. Pharm. Biopharm.* **2017**, *119*, 353−360.
(33) Badkar, A. V.; Gandhi, R.; Davis, S.; LaBarre, M. Subcutaneous delivery of high-dose/volume biologics: Current status and prospect for future advancements. *Drug Des., Dev. Ther.* **2021**, *15*, 159−170.
(34) Jogdeo, C. M.; Bhattacharya, D. S.; Lin, V.; Kolhe, P.; Badkar, A. Assessing physicochemical stability of monoclonal antibodies in a simulated subcutaneous environment. *J. Pharm. Sci.* **2024**, *113* (7), 1854−1864, DOI: 10.1016/j.xphs.2024.02.004.
(35) Le Basle, Y.; Chennell, P.; Tokhadze, N.; Astier, A.; Sautou, V. Physicochemical stability of monoclonal antibodies: A review. *J. Pharm. Sci.* **2020**, *109*, 169−190.
(36) Jiskoot, W.; Hawe, A.; Menzen, T.; Volkin, D. B.; Crommelin, D. J. Ongoing challenges to develop high concentration monoclonal antibody-based formulations for subcutaneous administration: Quo Vadis? *J. Pharm. Sci.* **2022**, *111*, 861−867.
(37) Andya, J. D.; Liu, J.; Shire, S. J. Analysis of Irreversible Aggregation, Reversible Self-Association and Fragmentation of Monoclonal Antibodies by Analytical Ultracentrifugation. In *Current Trends in Monoclonal Antibody Development and Manufacturing*, 2010; pp 207−227.
(38) Pang, K. T.; Yang, Y. S.; Zhang, W.; Ho, Y. S.; Sormanni, P.; Michaels, T. C.; Walsh, I.; Chia, S. Understanding and controlling the molecular mechanisms of protein aggregation in mAb therapeutics. *Biotechnol. Adv.* **2023**, *67*, No. 108192.
(39) Lao, Z.; Tang, Y.; Dong, X.; Tan, Y.; Li, X.; Liu, X.; Li, L.; Guo, C.; Wei, G. Elucidating the reversible and irreversible self-assembly mechanisms of low-complexity aromatic-rich kinked peptides and steric zipper peptides. *Nanoscale* **2024**, *16*, 4025−4038.
(40) Liu, J.; Nguyen, M. D.; Andya, J. D.; Shire, S. J. Reversible self-association increases the viscosity of a concentrated monoclonal antibody in aqueous solution. *J. Pharm. Sci.* **2005**, *94*, 1928−1940.
(41) Kanai, S.; Liu, J.; Patapoff, T. W.; Shire, S. J. Reversible self-association of a concentrated monoclonal antibody solution mediated by Fab-Fab interaction that impacts solution viscosity. *J. Pharm. Sci.* **2008**, *97*, 4219−4227.
(42) Yadav, S.; Liu, J.; Shire, S. J.; Kalonia, D. S. Specific interactions in high concentration antibody solutions resulting in high viscosity. *J. Pharm. Sci.* **2010**, *99*, 1152−1168.
(43) Binabaji, E.; Ma, J.; Zydney, A. L. Intermolecular interactions and the viscosity of highly concentrated monoclonal antibody solutions. *Pharm. Res.* **2015**, *32*, 3102−3109.
(44) Sukumar, M.; Doyle, B. L.; Combs, J. L.; Pekar, A. H. Opalescent appearance of an IgG1 antibody at high concentrations and its relationship to noncovalent association. *Pharm. Res.* **2004**, *21*, 1087−1093.
(45) Salinas, B. A.; Sathish, H. A.; Bishop, S. M.; Harn, N.; Carpenter, J. F.; Randolph, T. W. Understanding and modulating opalescence and viscosity in a monoclonal antibody formulation. *J. Pharm. Sci.* **2010**, *99*, 82−93.
(46) Mason, B. D.; Zhang, L.; Remmele, R. L., Jr.; Zhang, J. Opalescence of an IgG2 monoclonal antibody solution as it relates to liquid-liquid phase separation. *J. Pharm. Sci.* **2011**, *100*, 4587−4596.
(47) Raut, A. S.; Kalonia, D. S. Opalescence in monoclonal antibody solutions and its correlation with intermolecular interactions in dilute and concentrated solutions. *J. Pharm. Sci.* **2015**, *104*, 1263−1274.
(48) Arora, J.; Hu, Y.; Esfandiary, R.; Sathish, H. A.; Bishop, S. M.; Joshi, S. B.; Middaugh, C. R.; Volkin, D. B.; Weis, D. D. Charge-mediated Fab-Fc interactions in an IgG1 antibody induce reversible self-association, cluster formation, and elevated viscosity. *mAbs* **2016**, *8* (8), 1561−1574.
(49) Nakauchi, Y.; Nishinami, S.; Murakami, Y.; Ogura, T.; Kano, H.; Shiraki, K. Opalescence arising from network assembly in antibody solution. *Mol. Pharmaceutics* **2022**, *19*, 1160−1167.
(50) Kimball, W. D.; Lanzaro, A.; Hurd, C.; Jhaveri, N.; Huang, J.; Lewandowski, J.; Qian, K. K.; Woldeyes, M. A.; Majumdar, R.; Witek, M. A.; et al. Growth of Clusters toward Liquid-Liquid Phase Separation of Monoclonal Antibodies as Characterized by Small-Angle X-ray Scattering and Molecular Dynamics Simulation. *J. Phys. Chem. B* **2025**, *129* (11), 2856−2871, DOI: 10.1021/acs.jpcb.4c07064.
(51) Esfandiary, R.; Parupudi, A.; Casas-Finet, J.; Gadre, D.; Sathish, H. Mechanism of reversible self-association of a monoclonal antibody: role of electrostatic and hydrophobic interactions. *J. Pharm. Sci.* **2015**, *104* (2), 577−586.
(52) Kastelic, M.; Dill, K. A.; Kalyuzhnyi, Y. V.; Vlachy, V. Controlling the viscosities of antibody solutions through control of their binding sites. *J. Mol. Liq.* **2018**, *270*, 234−242.
(53) Li, L.; Kumar, S.; Buck, P. M.; Burns, C.; Lavoie, J.; Singh, S. K.; Warne, N. W.; Nichols, P.; Luksha, N.; Boardman, D. Concentration dependent viscosity of monoclonal antibody solutions: explaining experimental behavior in terms of molecular properties. *Pharm. Res.* **2014**, *31*, 3161−3178.
(54) Sharma, V. K.; Patapoff, T. W.; Kabakoff, B.; Pai, S.; Hilario, E.; Zhang, B.; Li, C.; Borisov, O.; Kelley, R. F.; Chorny, I.; Zhou, J. Z.; Dill, K. A.; Swartz, T. E. In silico selection of therapeutic antibodies for development: viscosity, clearance. *Proc. Natl. Acad. Sci. U.S.A.* **2014**, *111*, 18601−18606.
(55) Tomar, D. S.; Li, L.; Broulidakis, M. P.; Luksha, N. G.; Burns, C. T.; Singh, S. K.; Kumar, S. In-silico prediction of concentration-dependent viscosity curves for monoclonal antibody solutions. *mAbs* **2017**, *9* (3), 476−489.
(56) Apgar, J. R.; Tam, A. S.; Sorm, R.; Moesta, S.; King, A. C.; Yang, H.; Kelleher, K.; Murphy, D.; D'Antona, A. M.; Yan, G.; et al. Modeling and mitigation of high-concentration antibody viscosity through structure-based computer-aided protein design. *PLoS One* **2020**, *15*, No. e0232713.
(57) Lai, P.-K.; Ghag, G.; Yu, Y.; Juan, V.; Fayadat-Dilman, L.; Trout, B. L. Differences in human IgG1 and IgG4 S228P monoclonal antibodies viscosity and self-interactions: Experimental assessment and computational predictions of domain interactions. *mAbs* **2021**, *13* (1), No. 1991256.
(58) Blanco, M. A. Computational models for studying physical instabilities in high concentration biotherapeutic formulations. *mAbs* **2022**, *14*, No. 2044744.
(59) Forder, J. K.; Ilott, A. J.; Sahin, E.; Roberts, C. J. Simulation of high-concentration self-interactions for monoclonal antibodies from

well-behaved to poorly-behaved systems. *AIChE J.* **2023**, *69*, No. e17965.
(60) Humphrey, W.; Dalke, A.; Schulten, K. VMD: Visual Molecular Dynamics. *J. Mol. Graphics* **1996**, *14*, 33−38.
(61) Eargle, J.; Wright, D.; Luthey-Schulten, Z. Multiple Alignment of protein structures and sequences for VMD. *Bioinformatics* **2006**, *22*, 504−506.
(62) Larkin, M. A.; Blackshields, G.; Brown, N. P.; Chenna, R.; McGettigan, P. A.; McWilliam, H.; Valentin, F.; Wallace, I. M.; Wilm, A.; Lopez, R.; et al. Clustal W and Clustal X version 2.0. *Bioinformatics* **2007**, *23*, 2947−2948.
(63) Schmitt, J.; Razvi, A.; Grapentin, C. Predictive modeling of concentration-dependent viscosity behavior of monoclonal antibody solutions using artificial neural networks. *mAbs* **2023**, *15*, No. 2169440.
(64) Armstrong, G. B.; Shah, V.; Sanches, P.; Patel, M.; Casey, R.; Jamieson, C.; Burley, G. A.; Lewis, W.; Rattray, Z. A framework for the biophysical screening of antibody mutations targeting solvent-accessible hydrophobic and electrostatic patches for enhanced viscosity profiles. *Comput. Struct. Biotechnol. J.* **2024**, *23*, 2345−2357.
(65) Dai, J.; Izadi, S.; Zarzar, J.; Wu, P.; Oh, A.; Carter, P. J. Variable domain mutational analysis to probe the molecular mechanisms of high viscosity of an IgG1 antibody. *mAbs* **2024**, *16* (1), No. 2304282.
(66) Li, M.; Wang, Y.; Tao, F.; Xu, P.; Zhang, S. QTY code designed antibodies for aggregation prevention: A structural bioinformatic and computational study. *Proteins: Struct., Funct., Bioinf.* **2024**, *92*, 206−218.
(67) Makowski, E. K.; Chen, H.-T.; Tessier, P. M. Simplifying complex antibody engineering using machine learning. *Cell Syst.* **2023**, *14*, 667−675.
(68) Makowski, E. K.; Chen, H.-T.; Wang, T.; Wu, L.; Huang, J.; Mock, M.; Underhill, P.; Pelegri-O'Day, E.; Maglalang, E.; Winters, D.; Tessier, P. M. Reduction of monoclonal antibody viscosity using interpretable machine learning. *mAbs* **2024**, *16* (1), No. 2303781.
(69) Li, B.; Luo, S.; Wang, W.; Xu, J.; Liu, D.; Shameem, M.; Mattila, J.; Franklin, M. C.; Hawkins, P. G.; Atwal, G. S. PROPERMAB: an integrative framework for in silico prediction of antibody developability using machine learning. *mAbs* **2025**, *17*, No. 2474521.
(70) Wang, S.; Zhang, N.; Hu, T.; Dai, W.; Feng, X.; Zhang, X.; Qian, F. Viscosity-lowering effect of amino acids and salts on highly concentrated solutions of two IgG1 monoclonal antibodies. *Mol. Pharmaceutics* **2015**, *12*, 4478−4487.
(71) Yuan, G.; Salipante, P. F.; Hudson, S. D.; Gillilan, R. E.; Huang, Q.; Hatch, H. W.; Shen, V. K.; Grishaev, A. V.; Pabit, S.; Upadhya, R.; et al. Flow activation energy of high-concentration monoclonal antibody solutions and protein-protein interactions influenced by NaCl and sucrose. *Mol. Pharmaceutics* **2024**, *21*, 4553−4564.
(72) Dear, B. J.; Hung, J. J.; Truskett, T. M.; Johnston, K. P. Contrasting the influence of cationic amino acids on the viscosity and stability of a highly concentrated monoclonal antibody. *Pharm. Res.* **2017**, *34*, 193−207.
(73) Dear, B. J.; Hung, J. J.; Laber, J. R.; Wilks, L. R.; Sharma, A.; Truskett, T. M.; Johnston, K. P. Enhancing stability and reducing viscosity of a monoclonal antibody with cosolutes by weakening protein-protein interactions. *J. Pharm. Sci.* **2019**, *108*, 2517−2526.
(74) Tilegenova, C.; Izadi, S.; Yin, J.; Huang, C. S.; Wu, J.; Ellerman, D.; Hymowitz, S. G.; Walters, B.; Salisbury, C.; Carter, P. J. Dissecting the molecular basis of high viscosity of monospecific and bispecific IgG antibodies. *mAbs* **2020**, *12*, No. 1692764.
(75) Ye, Y.; Huo, X.; Yin, Z. Protein-protein interactions at high concentrations: Effects of ArgHCl and NaCl on the stability, viscosity and aggregation mechanisms of protein solution. *Int. J. Pharm.* **2021**, *601*, No. 120535.
(76) Guo, Z.; Chen, A.; Nassar, R. A.; Helk, B.; Mueller, C.; Tang, Y.; Gupta, K.; Klibanov, A. M. Structure-activity relationship for hydrophobic salts as viscosity-lowering excipients for concentrated solutions of monoclonal antibodies. *Pharm. Res.* **2012**, *29*, 3102−3109.
(77) Zeng, Y.; Tran, T.; Wuthrich, P.; Naik, S.; Davagnino, J.; Greene, D. G.; Mahoney, R. P.; Soan, S. D. Caffeine as a viscosity reducer for highly concentrated monoclonal antibody solutions. *J. Pharm. Sci.* **2021**, *110*, 3594−3604.
(78) Srivastava, A.; O'Dell, C.; Bolessa, E.; McLinden, S.; Fortin, L.; Deorkar, N. Viscosity reduction and stability enhancement of monoclonal antibody formulations using derivatives of amino acids. *J. Pharm. Sci.* **2022**, *111*, 2848−2856.
(79) Lapenna, A.; Dagallier, C.; Huille, S.; Tribet, C. Poly (glutamic acid)-based viscosity reducers for concentrated formulations of a monoclonal IgG antibody. *Mol. Pharmaceutics* **2024**, *21* (2), 982−991, DOI: 10.1021/acs.molpharmaceut.3c01159.
(80) Braun, S.; Banik, N.; Widera, J. J.; Brandenburg, J. G.; Rosenkranz, T. In The Viscosity Reduction Platform: Viscosity-Reducing Excipients for Protein Formulation, *MilliporeSigma White Paper*, 2021.
(81) Dear, B. J.; Chowdhury, A.; Hung, J. J.; Karouta, C. A.; Ramachandran, K.; Nieto, M. P.; Wilks, L. R.; Sharma, A.; Shay, T. Y.; Cheung, J. K.; et al. Relating collective diffusion, protein-protein interactions, and viscosity of highly concentrated monoclonal antibodies through dynamic light scattering. *Ind. Eng. Chem. Res.* **2019**, *58*, 22456−22471.
(82) Gentiluomo, L.; Roessner, D.; Streicher, W.; Mahapatra, S.; Harris, P.; Frieß, W. Characterization of native reversible self-association of a monoclonal antibody mediated by Fab-Fab interaction. *J. Pharm. Sci.* **2020**, *109*, 2517−2526.
(83) Skar-Gislinge, N.; Camerin, F.; Stradner, A.; Zaccarelli, E.; Schurtenberger, P. Using cluster theory to calculate the experimental structure factors of antibody solutions. *Mol. Pharmaceutics* **2023**, *20* (5), 2738−2753, DOI: 10.1021/acs.molpharmaceut.3c00191.
(84) Chowdhury, A.; Manohar, N.; Guruprasad, G.; Chen, A. T.; Lanzaro, A.; Blanco, M.; Johnston, K. P.; Truskett, T. M. Characterizing experimental monoclonal antibody interactions and clustering using a coarse-grained simulation library and a viscosity model. *J. Phys. Chem. B* **2023**, *127*, 1120−1137.
(85) Gulotta, A.; Polimeni, M.; Lenton, S.; Starr, C. G.; Stradner, A.; Zaccarelli, E.; Schurtenberger, P. Combining scattering experiments and colloid theory to characterize charge effects in concentrated antibody solutions. *Mol. Pharmaceutics* **2024**, *21* (5), 2250−2271, DOI: 10.1021/acs.molpharmaceut.3c01023.
(86) Polimeni, M.; Zaccarelli, E.; Gulotta, A.; Lund, M.; Stradner, A.; Schurtenberger, P. A multi-scale numerical approach to study monoclonal antibodies in solution. *APL Bioeng.* **2024**, *8*, No. 016111, DOI: 10.1063/5.0186642.
(87) Saurabh, S.; Zhang, Q.; Seddon, J. M.; Lu, J. R.; Kalonia, C.; Bresme, F. Unraveling the microscopic mechanism of molecular ion interaction with monoclonal antibodies: impact on protein aggregation. *Mol. Pharmaceutics* **2024**, *21*, 1285−1299.
(88) Mosca, I.; Pounot, K.; Beck, C.; Colin, L.; Matsarskaia, O.; Grapentin, C.; Seydel, T.; Schreiber, F. Biophysical determinants for the viscosity of concentrated monoclonal antibody solutions. *Mol. Pharmaceutics* **2023**, *20*, 4698−4713.
(89) Brudar, S.; Breydo, L.; Chung, E.; Dill, K. A.; Ehterami, N.; Phadnis, K.; Senapati, S.; Shameem, M.; Tang, X.; Tayyab, M.; Hribar-Lee, B. Antibody association in solution: cluster distributions and mechanisms. *mAbs* **2024**, *16* (1), No. 2339582.
(90) Yearley, E. J.; Godfrin, P. D.; Perevozchikova, T.; Zhang, H.; Falus, P.; Porcar, L.; Nagao, M.; Curtis, J. E.; Gawande, P.; Taing, R.; et al. Observation of small cluster formation in concentrated monoclonal antibody solutions and its implications to solution viscosity. *Biophys. J.* **2014**, *106*, 1763−1770.
(91) Zhai, Y.; Martys, N. S.; George, W. L.; Curtis, J. E.; Nayem, J.; Z, Y.; Liu, Y. Intermediate scattering functions of a rigid body monoclonal antibody protein in solution studied by dissipative particle dynamic simulation. *Struct. Dyn.* **2021**, *8*, No. 024102, DOI: 10.1063/4.0000086.
(92) Godfrin, P. D.; Zarraga, I. E.; Zarzar, J.; Porcar, L.; Falus, P.; Wagner, N. J.; Liu, Y. Effect of hierarchical cluster formation on the

viscosity of concentrated monoclonal antibody formulations studied by neutron scattering. *J. Phys. Chem. B* **2016**, *120*, 278−291.
(93) Stingaciu, L. R.; Ivanova, O.; Ohl, M.; Biehl, R.; Richter, D. Fast antibody fragment motion: flexible linkers act as entropic spring. *Sci. Rep.* **2016**, *6*, No. 22148.
(94) Sohmen, B.; Beck, C.; Frank, V.; Seydel, T.; Hoffmann, I.; Hermann, B.; Nüesch, M.; Grimaldo, M.; Schreiber, F.; Wolf, S.; Roosen-Runge, F.; Hugel, T. The onset of molecule-spanning dynamics in Heat Shock Protein Hsp90. *Adv. Sci.* **2023**, *10*, No. 2304262.
(95) Girelli, A.; Beck, C.; Bäuerle, F.; Matsarskaia, O.; Maier, R.; Zhang, F.; Wu, B.; Lang, C.; Czakkel, O.; Seydel, T.; Schreiber, F.; Roosen-Runge, F. Molecular Flexibility of Antibodies Preserved Even in the Dense Phase after Macroscopic Phase Separation. *Mol. Pharmaceutics* **2021**, *18*, 4162−4169.
(96) Huber, R.; Deisenhofer, J.; Colman, P. M.; Matsushima, M.; Palm, W. Crystallographic structure studies of an IgG molecule and an Fc fragment. *Nature* **1976**, *264*, 415−420.
(97) Saphire, E. O.; Parren, P. W.; Pantophlet, R.; Zwick, M. B.; Morris, G. M.; Rudd, P. M.; Dwek, R. A.; Stanfield, R. L.; Burton, D. R.; Wilson, I. A. Crystal structure of a neutralizing human IgG against HIV-1: a template for vaccine design. *Science* **2001**, *293*, 1155−1159.
(98) Aalberse, R. C.; Schuurman, J. IgG4 breaking the rules. *Immunology* **2002**, *105*, 9−19.
(99) Newman, R.; Hariharan, K.; Reff, M.; Anderson, D. R.; Braslawsky, G.; Santoro, D.; Hanna, N.; Bugelski, P. J.; Brigham-Burke, M.; Crysler, C.; et al. Modification of the Fc region of a primatized IgG antibody to human CD4 retains its ability to modulate CD4 receptors but does not deplete CD4+ T cells in chimpanzees. *Clin. Immunol.* **2001**, *98*, 164−174.
(100) Roux, K. H.; Strelets, L.; Michaelsen, T. E. Flexibility of human IgG subclasses. *J. Immunol.* **1950**, *1997* (159), 3372−3382.
(101) Shambesh, M.; Craig, P.; Wen, H.; Rogan, M.; Paolillo, E. IgG1 and IgG4 serum antibody responses in asymptomatic and clinically expressed cystic echinococcosis patients. *Acta Trop.* **1997**, *64*, 53−63.
(102) Neergaard, M. S.; Kalonia, D. S.; Parshad, H.; Nielsen, A. D.; Møller, E. H.; Van De Weert, M. Viscosity of high concentration protein formulations of monoclonal antibodies of the IgG1 and IgG4 subclass-Prediction of viscosity through protein-protein interaction measurements. *Eur. J. Pharm. Sci.* **2013**, *49*, 400−410.
(103) Scarcelli, J. J.; Shang, T. Q.; Iskra, T.; Allen, M. J.; Zhang, L. Strategic deployment of CHO expression platforms to deliver Pfizer's Monoclonal Antibody Portfolio. *Biotechnol. Prog.* **2017**, *33*, 1463−1467.
(104) Wang, S. S.; Yan, Y. S.; Ho, K. US FDA-approved therapeutic antibodies with high-concentration formulation: summaries and perspectives. *Antibody Ther.* **2021**, *4*, 262−272.
(105) Covington, A. K.; Paabo, M.; Robinson, R. A.; Bates, R. G. Use of the glass electrode in deuterium oxide and the relation between the standardized pd (pad) scale and the operational pH in heavy water. *Anal. Chem.* **1968**, *40*, 700−706.
(106) De Gennes, P. G. Dynamics of entangled polymer solutions. I. The Rouse model. *Macromolecules* **1976**, *9*, 587−593.
(107) Hoffmann, I. Data analysis and background subtraction in Neutron Spin Echo spectroscopy. *Front. Phys.* **2021**, *8*, No. 620082.
(108) Lindner, P.; Schweins, R. The D11 small-angle scattering instrument: A new benchmark for SANS. *Neutron News* **2010**, *21*, 15−18.
(109) Klosowski, P.; Koennecke, M.; Tischler, J.; Osborn, R. NeXus: A common format for the exchange of neutron and synchrotron data. *Phys. B* **1997**, *241*−*243*, 151−153.
(110) Könnecke, M.; Akeroyd, F. A.; Bernstein, H. J.; Brewster, A. S.; Campbell, S. I.; Clausen, B.; Cottrell, S.; Hoffmann, J. U.; Jemian, P. R.; Männicke, D.; et al. NeXus data format. *J. Appl. Crystallogr.* **2015**, *48*, 301−305.
(111) Dewhurst, C. D. Graphical reduction and analysis small-angle neutron scattering program: GRASP. *J. Appl. Crystallogr.* **2023**, *56*, 1595−1609.
(112) Gowers, R. J.; Linke, M.; Barnoud, J.; Reddy, T. J. E.; Melo, M. N.; Seyler, S. L.; Domański, J.; Dotson, D. L.; Buchoux, S.; Kenney, I. M.; Beckstein, O. In *MDAnalysis: A Python Package for the Rapid Analysis of Molecular Dynamics Simulations*, Proceedings of the 15th Python in Science Conference, 2016; pp 98−105.
(113) Kingsbury, J. S.; Saini, A.; Auclair, S. M.; Fu, L.; Lantz, M. M.; Halloran, K. T.; Calero-Rubio, C.; Schwenger, W.; Airiau, C. Y.; Zhang, J.; Gokarn, Y. R. A single molecular descriptor to predict solution behavior of therapeutic antibodies. *Sci. Adv.* **2020**, *6*, No. eabb0372.
(114) Banchio, A. J.; Nägele, G. Short-time transport properties in dense suspensions: from neutral to charge-stabilized colloidal spheres. *J. Chem. Phys.* **2008**, *128*, No. 104903.
(115) Inoue, R.; Oroguchi, T.; Oda, T.; Farago, B.; Martel, A.; Porcar, L.; Sato, M.; Sugiyama, M. Internal dynamics of multidomain protein as revealed by an optimized neutron spin echo measurement and all-atom molecular dynamics simulation. *Phys. Rev. Res.* **2023**, *5*, No. 043154.
(116) Biehl, R. Jscatter, a program for evaluation and analysis of experimental data. *PLoS One* **2019**, *14*, No. e0218789.
(117) Nägele, G. On the dynamics and structure of charge-stabilized suspensions. *Phys. Rep.* **1996**, *272*, 215−372.
(118) Raut, A. S.; Kalonia, D. S. Liquid-Liquid phase separation in a dual variable domain immunoglobulin protein solution: effect of formulation factors and protein-protein interactions. *Mol. Pharmaceutics* **2015**, *12*, 3261−3271.
(119) Yang, T.-C.; Langford, A. J.; Kumar, S.; Ruesch, J. C.; Wang, W. Trimerization dictates solution opalescence of a monoclonal antibody. *J. Pharm. Sci.* **2016**, *105*, 2328−2337.
(120) Chowdhury, A. A.; Manohar, N.; Witek, M. A.; Woldeyes, M. A.; Majumdar, R.; Qian, K. K.; Kimball, W. D.; Xu, S.; Lanzaro, A.; Truskett, T. M.; Johnston, K. P. Subclass effects on self-association and viscosity of monoclonal antibodies at high concentrations. *Mol. Pharmaceutics* **2023**, *20*, 2991−3008.
(121) Natesan, R.; Agrawal, N. J. Non-covalent Fc-Fab interactions significantly alter internal dynamics of an IgG1 antibody. *Sci. Rep.* **2022**, *12*, No. 9321.
(122) Koppel, D. E. Analysis of macromolecular polydispersity in intensity correlation spectroscopy: the method of cumulants. *J. Chem. Phys.* **1972**, *57*, 4814−4820.
(123) Frisken, B. J. Revisiting the method of cumulants for the analysis of dynamic light-scattering data. *Appl. Opt.* **2001**, *40*, 4087−4091.
(124) Odhner, H.; Jacobs, D. Refractive index of liquid D2O for visible wavelengths. *J. Chem. Eng. Data* **2012**, *57*, 166−168.
(125) Pedersen, J. S. Analysis of small-angle scattering data from colloids and polymer solutions: modeling and least-squares fitting. *Adv. Colloid Interface Sci.* **1997**, *70*, 171−210.
(126) Lindner, P.; Zemb, T. *Neutrons, X-rays, and Light: Scattering Methods Applied to Soft Condensed Matter*; Elsevier: North-Holland, 2002.
(127) Debye, P. Zerstreuung von Röntgenstrahlen. *Ann. Phys.* **1915**, *351*, 809−823.
(128) Hansen, J.-P.; McDonald, I. R. *Theory of Simple Liquids*, 3rd ed.; Academic Press: Amsterdam, 2006.
(129) Feigin, L. A.; Svergun, D. I. *Structure Analysis by Small-Angle X-Ray and Neutron Scattering*; Plenum Press: New York, 1987.
(130) Guinier, A.; Fournet, G. *Small-Angle Scattering of X-rays*; Wiley: New York, 1955; Vol. *14*.
(131) Imamura, H.; Ooishi, A.; Honda, S. Getting smaller by denaturation: acid-induced compaction of antibodies. *J. Phys. Chem. Lett.* **2023**, *14*, 3898−3906.
(132) Calero-Rubio, C.; Ghosh, R.; Saluja, A.; Roberts, C. J. Predicting protein-protein interactions of concentrated antibody solutions using dilute solution data and coarse-grained molecular models. *J. Pharm. Sci.* **2018**, *107*, 1269−1281.
(133) Bhandari, K.; Wei, Y.; Amer, B. R.; Pelegri-O'Day, E. M.; Huh, J.; Schmit, J. D. Prediction of Antibody Viscosity from Dilute Solution

Measurements. *Antibodies* **2023**, *12*, No. 78, DOI: 10.3390/antib12040078.
(134) Mosca, I.; Beck, C.; Grapentin, C.; Grundel, A.; Hoffmann, I.; Matsarskaia, O.; Nasro, R.; Pounot, K.; Schreiber, F.; Seydel, T. Differences between Monoclonal Antibodies: Viscosity, Diffusion, and Transient Cluster Formation, 2023. https://doi.ill.fr/10.5291/ILL-DATA.8-04-932.

https://doi.org/10.1021/acs.molpharmaceut.5c00327
Mol. Pharmaceutics 2025, 22, 5373−5388